FOI
SWEDISH DEFENCE
RESEARCH AGENCY

FOI-R--0425--SE
February 2002
ISSN 1650-1942
Technical report

Stefan Silfverskiöld, Mats Bäckström, Jörgen Lorén

Microwave Field-to-Printed-Circuit-Board Coupling Measurements in Reverberation Chamber

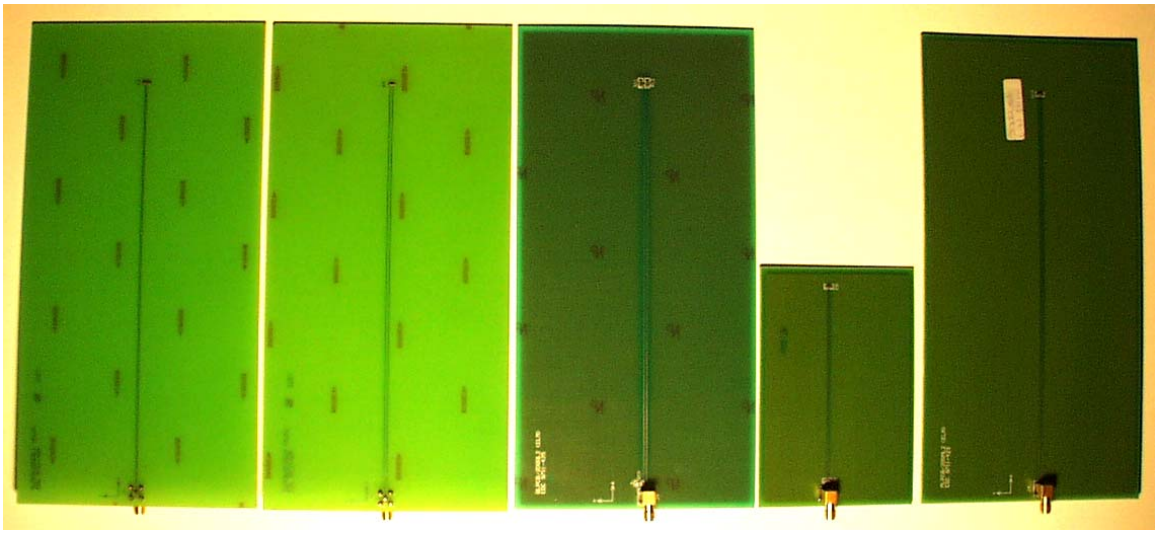

Sensor Technology
SE-581 11 Linköping

SWEDISH DEFENCE RESEARCH AGENCY

Sensor Technology
P.O. Box 1165
SE-581 11 Linköping

FOI-R--0425--SE

February 2002

ISSN 1650-1942

Technical report

Stefan Silfverskiöld, Mats Bäckström, Jörgen Lorén

Microwave Field-to-Printed-Circuit-Board Coupling Measurements in Reverberation Chamber

Issuing organization	Report number, ISRN	Report type
FOI – Swedish Defence Research Agency Sensor Technology P.O. Box 1165 SE-581 11 Linköping	FOI-R--0425--SE	Technical report
	Research area code 6. Electronic Warfare	
	Month year February 2002	**Project no.** E 3031
	Customers code 5. Contracted Research	
	Sub area code 61 Electronic Warfare, Electromagnetic Weapons	

Author/s (editor/s)	Project manager
Stefan Silfverskiöld Mats Bäckström Jörgen Lorén	Mats Bäckström
	Approved by
	Sponsoring agency Swedish Armed Forces
	Scientifically and technically responsible

Report title

Microwave Field-to-Printed-Circuit-Board Coupling Measurements in Reverberation Chamber

Abstract (not more than 200 words)

We have recently reported an experimental study of microwave, 0.5 to 18 GHz, field-to-wire coupling for some basic wire geometries above a ground plane performed in Anechoic (AC) and Reverberation Chambers (RC). Receiving parameters and comparisons between measurements in the two chambers were presented. We showed e.g. that the antenna receiving cross section σ_w of wires measured in the RC follows a χ^2-distribution with two degrees of freedom. In this report we study the field-to-printed-circuit-board coupling for some single-sided, double-sided and multi-layer printed-circuit-boards (PCBs) performed in RC. We present receiving parameters including the realized gain G_R, the impedance mismatch factor q, the input resistance R_{in}, the receiving cross section σ_w and the effective antenna length h_e. We show that σ_w of traces on PCBs also follows a χ^2-distribution with two degrees of freedom. The effective antenna length h_e of traces on PCBs is found to be bounded by the wave length λ. The impedance matched receiving cross section is bounded by $\lambda^2/8\pi$.

Keywords

HPM, EMC, Reverberation chamber, Microwaves, Field-to-Printed-Circuit-Board Coupling

Further bibliographic information	Language English
ISSN 1650-1942	**Pages** 56 p
	Price acc. to pricelist **Security classification**

Utgivare	Rapportnummer, ISRN	Klassificering
Totalförsvarets Forskningsinstitut - FOI	FOI-R--0425--SE	Teknisk rapport
Sensorteknik	**Forskningsområde**	
Box 1165	6. Telekrig	
581 11 Linköping	**Månad, år**	**Projektnummer**
	Februari 2002	E 3031
	Verksamhetsgren	
	5. Uppdragsfinansierad verksamhet	
	Delområde	
	61 Telekrigföring med EM-vapen och skydd	

Författare/redaktör	Projektledare
Stefan Silfverskiöld	Mats Bäckström
Mats Bäckström	**Godkänd av**
Jörgen Lorén	
	Uppdragsgivare/kundbeteckning
	Försvarsmakten, HKV
	Tekniskt och/eller vetenskapligt ansvarig

Rapportens titel (i översättning)

Mätning av koppling av mikrovågor till kretskort i modväxlande kammare

Sammanfattning (högst 200 ord)

Vi har nyligen rapporterat en studie av koppling av mikrovågor, 0.5 till 18 GHz, till ledare över ett jordplan genomförd såväl i modväxlande kammare (MVK) som i ekofri mäthall. Kopplingsparametrar och jämförelser mellan mätningar i de två kamrarna presenterades. Såväl varianstest som ”goodness-of-fit” test visade att kopplingsdata (mottagningstvärsnittet σ_w) från MVK’n är χ^2-fördelade med två frihetsgrader, utom nära 0.5 GHz. Denna rapport presenterar en studie av koppling av mikrovågor till några olika kretskort genomförd i MVK. De kretskort som studerats är enkelsidiga, dubbelsidiga och flerlager kort. Vi presenterar kopplingsparametrar, såsom realiserad antennvinst G_R, impedansanpassningsfaktorn q, inresistansen R_{in}, mottagningstvärsnittet σ_w och den effektiva antennlängden h_e för de kretskort som studerats. Vi visar att mottagningstvärsnittet σ_w uppmätt i MVK är χ^2-fördelad med två frihetsgrader. Den effektiva antennlängden h_e för ledningarna på kretskorten begränsas av våglängden λ. Det impedansanpassade mottagningstvärsnittet σ_w begränsas av kurvan $\lambda^2/8\pi$.

Nyckelord

HPM, EMC, Modväxlande kammare, Mikrovågor, Koppling till kretskort

Övriga bibliografiska uppgifter	Språk Engelska

ISSN 1650-1942	Antal sidor: 56 s.
Distribution enligt missiv	Pris: Enligt prislista
	Sekretess

CONTENTS

1 Introduction

We have recently reported a study of microwave field-to-wire coupling measurements for some simple wire geometries over a ground plane performed in anechoic (AC) and reverberation chambers (RC) [1, 2]. Results for receiving parameters such as the realized gain G_R, the antenna receiving cross section σ_w and the effective antenna length of the wire, h_e, were presented. We found that the ratio between the maximum and average values of G_R may exceed 15 dB in the AC, the average being equal to G_R measured in the RC. Furthermore, G_R measured in the RC was found to follow a χ^2-distribution with two degrees of freedom. The measurements of G_R in the AC did not follow the same distribution.

We are interested in knowing the receiving parameters for printed-circuit boards in order to make analyses of system susceptibilities based on component susceptibility data. In this report we therefore present results for microwave field-to-printed-circuit-board coupling measurements for some single-sided, double-sided and multi-layer printed-circuit-boards (PCBs) performed in reverberation chamber, see Fig. 1.

Fig. 1. Measurement of microwave coupling to a PCB in the reverberation chamber at FOI. The dimensions of the RC is 5.10 m * 2.46 m * 3.00 m. In the foreground the transmitting antenna is seen. The PCB is on top of the left styrofoam cylinder.

One of the activities of the HPM (High Power Microwave) project at the Swedish Defence Research Agency FOI has been to find and evaluate simple analytical expressions describing the coupling of microwaves into electronic enclosures. One conclusion is that the average shielding effectiveness (SE) of enclosures that are not electrically small [3, 4] can be estimated by:

$$\langle SE \rangle = \frac{2\pi \cdot V}{\sigma_a \cdot \lambda \cdot Q} \qquad (1)$$

where V is the volume, Q the quality factor of the enclosure, λ the wavelength and σ_a denotes the transmission cross section of the apertures causing the leakage of microwave radiation into the shielded enclosure. The average of SE is taken over different locations inside the enclosure.

Since it is not possible to derive σ_a from a comparative measurement of IEEE Std 299 type we have developed methods both to measure and calculate it [5, 6, 7 and 8]. Another HPM activity at FOI deals with the study of the susceptibility of electronic components to microwaves expressed in terms of the amount of microwave power absorbed by the component [9].

To be able to make analyses of system susceptibilities based on component susceptibility data and knowledge of internal field levels given by Eq. (1) we also need to determine the power picked up by traces on PCBs connected to the components.

The approach is to regard the traces on the PCBs as receiving antennas, where the antenna receiving cross section, σ_w, is defined by:

$$\sigma_w = \frac{P_{load}}{S_{inc}} \tag{2}$$

where P_{load} is the power received by the load and S_{inc} is the power density of the incident field.

For an antenna, σ_w is given by [3]:

$$\sigma_w = \frac{\lambda^2}{4\pi} \cdot G(\theta,\phi) \cdot p(\xi) \cdot q = \frac{\lambda^2}{4\pi} \cdot D(\theta,\phi) \cdot \eta \cdot p(\xi) \cdot q = \frac{\lambda^2}{4\pi} \cdot G_R(\theta,\phi,\xi) \tag{3}$$

where G is the gain, p the polarization mismatch factor and $q = 1 - |S_{11}|^2$ is the impedance mismatch factor and S_{11} is the reflection factor, measured with a Network Analyzer (NA).
D is the directivity and η the antenna efficiency, representing the ohmic losses (η = 1 for the lossless case). In the statistically isotropic environment of the RC the following relations hold: $\langle D \rangle = 1$ and $\langle p \rangle = ½$, cf. [10].

P_{load} in the RC is defined as:

$$\langle P_{load} \rangle = \frac{G_R \cdot \langle S_{inc} \rangle \cdot \lambda^2}{4\pi} \tag{4}$$

where the average is taken over all stirrer positions. $\langle S_{inc} \rangle$ is given by [10]:

$$\langle S_{inc} \rangle = \frac{8\pi}{\lambda^2} \cdot \langle P_{rec} \rangle \tag{5}$$

where P_{rec} is the power received by the field calibration antenna (assumed to be lossless and well matched). The calibration antenna (log periodic antenna from Condor), however, was found to have losses.

A correction function for this calibration antenna has been found according to [11]:

$$loss(f) = -0.0019 \cdot f^2 + 0.1549 \cdot f + 0.7957 \quad \text{[dB]} \quad (6)$$

Inserting $\langle S_{inc} \rangle$ in Eq. (5) into Eq. (4) a realized gain, G_R, can be derived for the RC measurements:

$$G_R = \frac{\langle P_{load} \rangle}{2 \cdot \langle P_{rec} \rangle} \quad (7)$$

Correcting for the losses in the calibration antenna (Eq. 6), we get:

$$G_R(f) = G_{R,uncorr}(f) - loss(f) \quad \text{[dB]} \quad (8)$$

We define, at each frequency; the impedance matched antenna receiving cross section $\hat{\sigma}_w$ as:

$$\hat{\sigma}_w(f) = \frac{\sigma_w(f)}{q(f)} \quad (9)$$

$\hat{\sigma}_w$ represents the maximum power that, at each frequency, can be delivered to a (matched) load.

A related parameter of interest is the effective antenna length of the trace on the PCB, h_e. It provides an understanding of how large fraction of the trace that effectively acts as a receiving antenna. h_e is defined as [3]:

$$h_e = \frac{V_{oc}}{E_{inc}} = \sqrt{\frac{4\sigma_w R_{in}}{qZ_0}} = \sqrt{\frac{\lambda^2}{\pi^2}\frac{G_R R_{in}}{120q}} \quad (10)$$

where V_{oc} is the open circuit voltage, E_{inc} is the incident electric field strength, $Z_0 \approx 120\pi$ is the free space wave impedance and R_{in} is the input resistance of the wire, derived from:

$$R_{in} = \mathrm{Re}\left(50 \cdot \frac{1+S_{11}}{1-S_{11}}\right) \quad (11)$$

We here present some typical examples of the receiving parameters G_R, q, R_{in}, σ_w and h_e for the PCBs that were studied. In the Appendices A-F the complete sets of plots for each PCB are given.

2 Results

The measurements were carried out in the FOI large Reverberation Chamber (RC), which has the dimensions 5.10 m * 2.46 m * 3.00 m [12, 19]. An HP 8510C Network Analyzer with HP 8517B S-parameter test set was used for the measurements. To avoid rotational symmetry the stirrers in the RC are folded. The microwave coupling, for frequencies between 0.5 and 18 GHz, to six different printed circuit boards (single-sided, double-sided and multi-layer) according to table 1 and Fig. 2 was studied. The PCBs have kindly been provided by the Defense Science Organisation (DSO) in Singapore.

Table 1. Description of the different PCBs that were studied. In the denotation of the load resistances, *n* stands for near end and *f* for far end, se text.

PCB type	Length [mm]	Trace separation	Load Resistance
SSPCB (200SL1)	200	20 mil (0.508 mm)	Z_{1n}=50 Ω, Z_{1f}=10 kΩ
SSPCB (200SL2)	200	50 mil (1.70 mm)	Z_{1n}=50 Ω, Z_{1f}=240 Ω
DSPCB (100DL1)	100	20 mil (0.508 mm)	Z_{1n}=50 Ω, Z_{1f}=12 kΩ Z_{2n}=27 Ω, Z_{2f}=12 kΩ
DSPCB (200DL2)	200	50 mil (1.70 mm)	Z_{1n}=50 Ω, Z_{1f}=12 kΩ, Z_{2n}=27 Ω, Z_{2f}=12 kΩ
MLPCB (100ML1)	100	20 mil (0.508 mm)	Z_{1n}=50 Ω, Z_{1f}=12 kΩ Z_{2n}=36 Ω, Z_{2f}=15 kΩ
MLPCB (200ML2)	200	50 mil (1.70 mm)	Z_{1n}=50 Ω, Z_{1f}=91 Ω Z_{2n}=36 Ω, Z_{2f}=15 kΩ

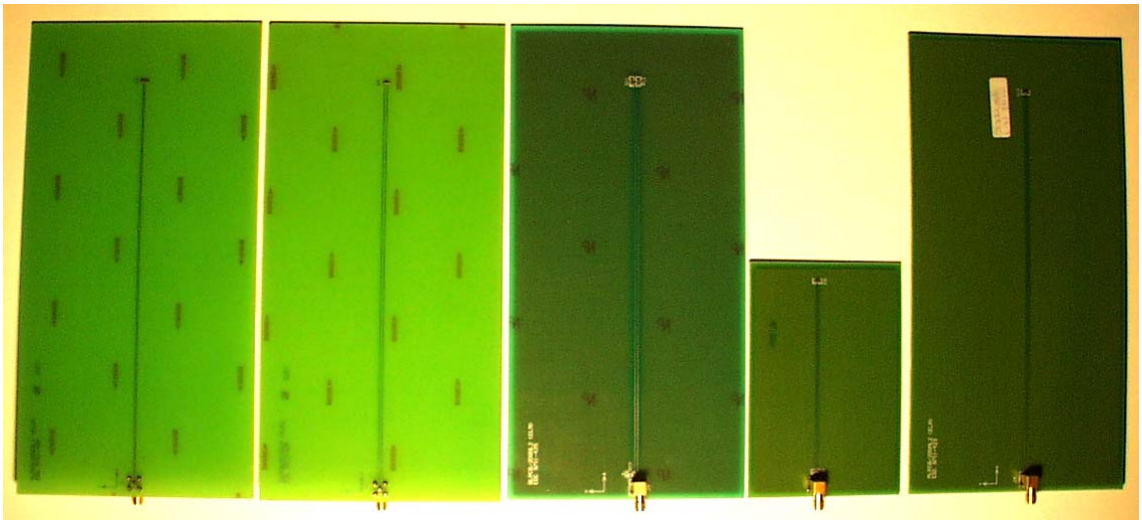

Fig. 2. The PCBs that were studied. (The double-sided PCB, pcb100dl1, is missing on the photo.)

2.1 Single-sided PCBs

Two copper traces are etched on the top of a single-sided PCB, with trace line width 10 mil (i.e. 0.254 mm), trace thickness 1 oz[1] (i.e. 34 μm Cu) and trace length 200 mm. The trace separation is 20 mil (i.e. 0.508 mm) for pcb200sl1 and 50 mil (i.e. 1.270 mm) for pcb200sl2. The thickness of the dielectric substrate is 1.6 mm and the dielectric constant ε_r, normally measured at 10 MHz, is ε_r = 4.7. At the near end of the traces an SMA jack is mounted between the two traces to connect the measurement equipment (50 Ω). At the far end of the traces a chip resistor is mounted between the traces according to Table 1. A circuit diagram and a cross section figure for the single-sided PCBs are given in Appendix A, page A0.

[1] 1 oz refers to the thickness you get when the given amount of copper is rolled out over an area of one square foot. This corresponds approximately to the thickness 34 μm.

In figure 3 the realized gain for pcb200sl1 is shown.

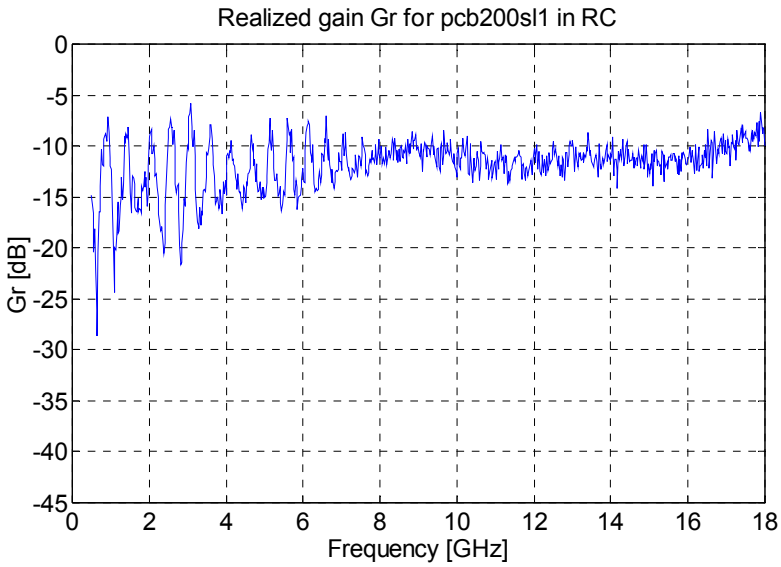

Fig. 3. Realized gain G_R for pcb200sl1.

Fig. 4 shows the realized gain G_R for pcb200sl2. We see in Figs. 3 and 4 that the realized gain looks qualitatively the same for these two PCBs.

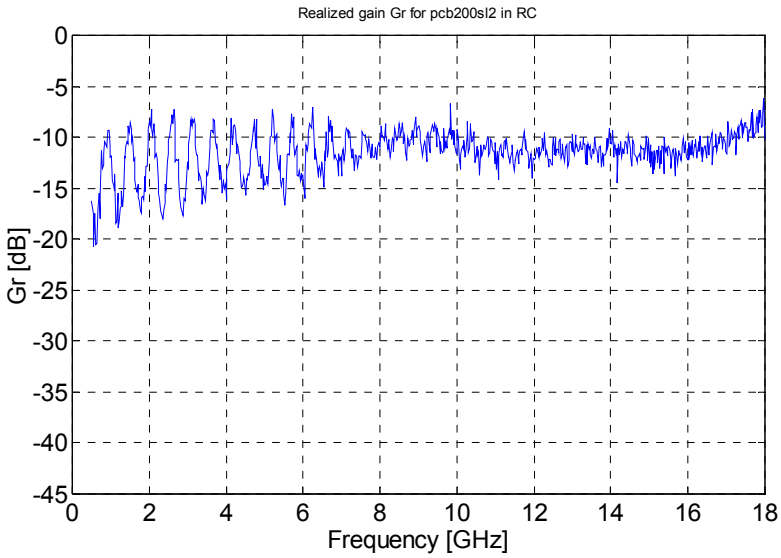

Fig. 4. Realized gain G_R for pcb200sl2.

Fig.5 shows the impedance matched receiving cross section for pcb200sl1 according to Eq. (9). The theoretical bounding curve $\lambda^2/8\pi$ is also plotted.

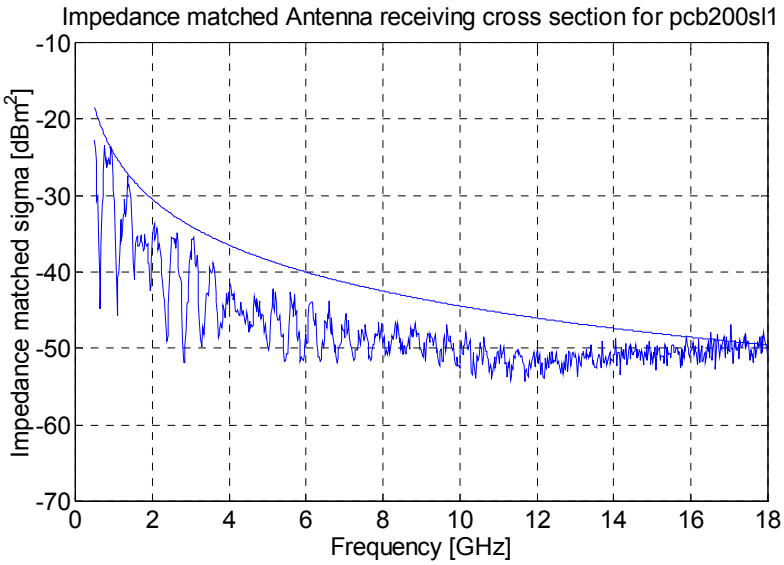

Fig. 5. Impedance matched receiving cross section for pcb200sl1 together with the bounding curve $\lambda^2/8\pi$.

2.2 Double-sided PCBs

Two copper traces are etched on one side of the double-sided PCB. The other side of the PCB is the ground plane. The parameters of the traces and dielectric substrate are the same as for the single sided PCB. At the near end of one of the traces an SMA connector is mounted. The other ends of the traces are terminated with chip resistors according to Table 1. On pcb100dl1 the trace length is 100 mm and the trace separation is 20 mil. The trace length on pcb200dl2 is 200 mm and the trace separation is 50 mil. For circuit diagram and cross section figure, see Appendix C.

Fig. 6 shows the realized gain G_R for pcb100dl1.

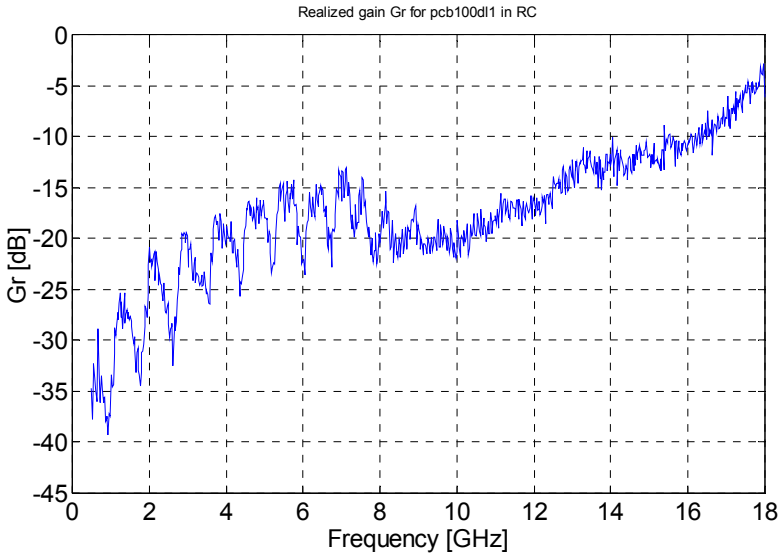

Fig. 6. Realized gain G_R for pcb100dl1.

Fig. 7 shows the realized gain for pcb200dl2. Fig. 6 and 7 show that the two double-sided PCBs qualitatively have the same frequency dependence of the realized gain.

The frequency step between the successive maxima in the range 0.5 to 6 GHz seen for pcb200dl2 is $\Delta f \approx 0.45$ GHz and for pcb100dl1 $\Delta f \approx 0.8$. This can presumably be explained by the fact that the trace length of pcb200 dl2 is twice as large as it is for pcb100dl1. Note that the step in wavelength is affected by the dielectric constant of the substrate, ε_r.

Comparing the realized gain of these two double sided PCBs with those of the single-sided PCBs shown in Fig. 3 and 4 we see that in the range 0.5 to 7 GHz the peaks for the double-sided PCBs are in the same order as the minima of the single-sided PCBs. In the range 8 to 12 GHz the realized gain of the double-sided PCBs are about 5 dB lower than for the single-sided PCBs. Above 12 GHz the realized gain for the double-sided PCBs increases rapidly so that at 18 GHz it is about 5 dB higher than for the single-sided PCBs.

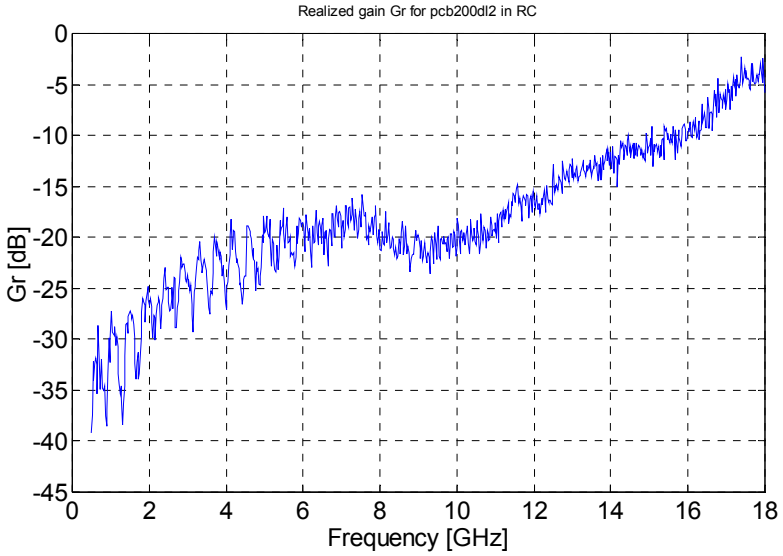

Fig. 7. Realized gain G_R for pcb200dl2.

The reflection factor S_{11} for pcb200dl2 is shown in Fig. 8.

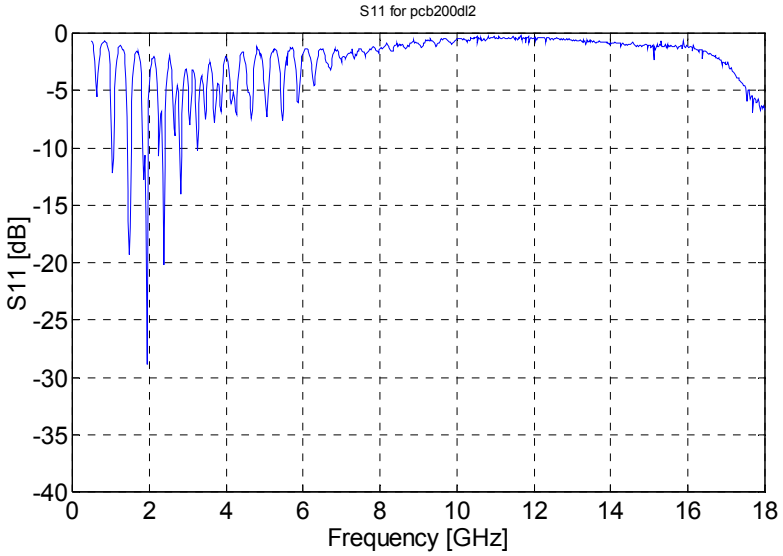

Fig. 8. The reflection factor S_{11} for pcb200dl2.

In Fig. 9 we show the impedance mismatch factor q for pcb200dl2.

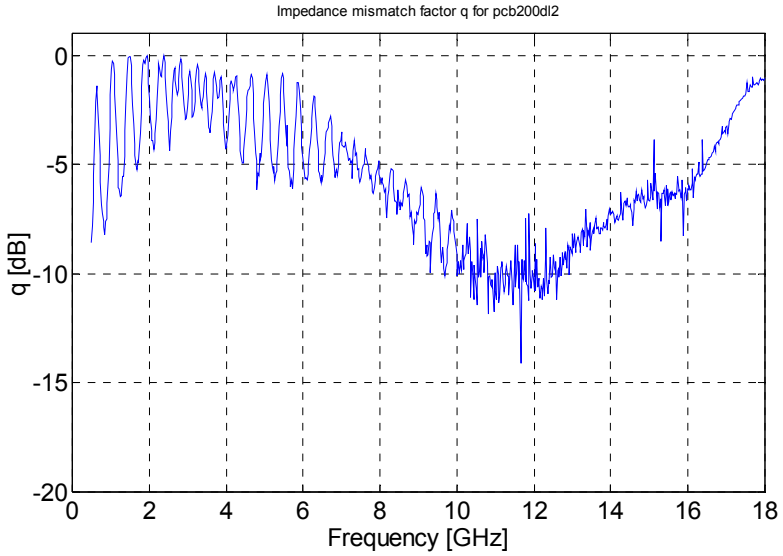

Fig. 9. Impedance mismatch factor q for pcb200dl2.

Fig. 10 shows the measured input resistance R_{in} according to Eq. (11) for pcb200dl2. In [2] we showed, with a simulation according to simple analytical expressions for a wire above a ground plane according to King [13], that the slowly varying structure of R_{in} for wires above a ground plane comes from the impedance transformation due to the SMA-jack at the near and far end of the wire. Since the structure of R_{in} in Fig. 10 is qualitatively similar to the measured R_{in} for a wire above a ground plane, we presume that the slowly varying structure in Fig. 10 comes from the SMA-jack at the near end of the PCB.

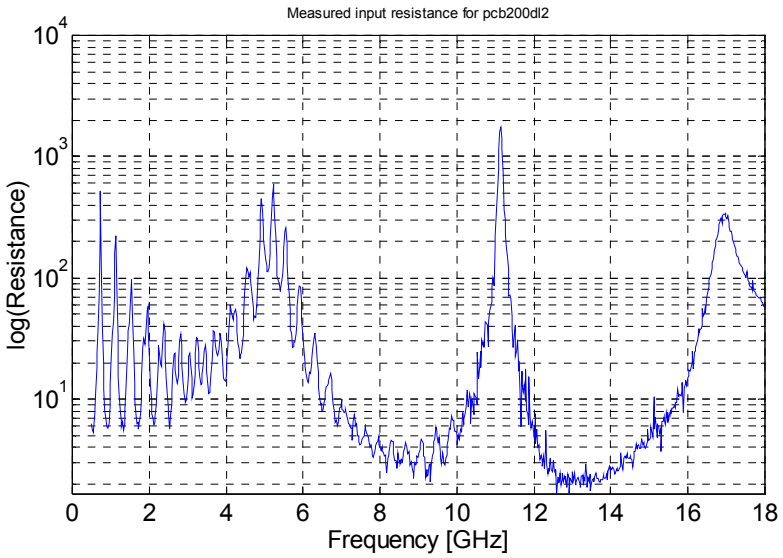

Fig. 10. The measured input resistance R_{in} for pcb200dl2.

The receiving cross section σ_w according to Eq. (3) for pcb200dl2 is shown in Fig. 11.

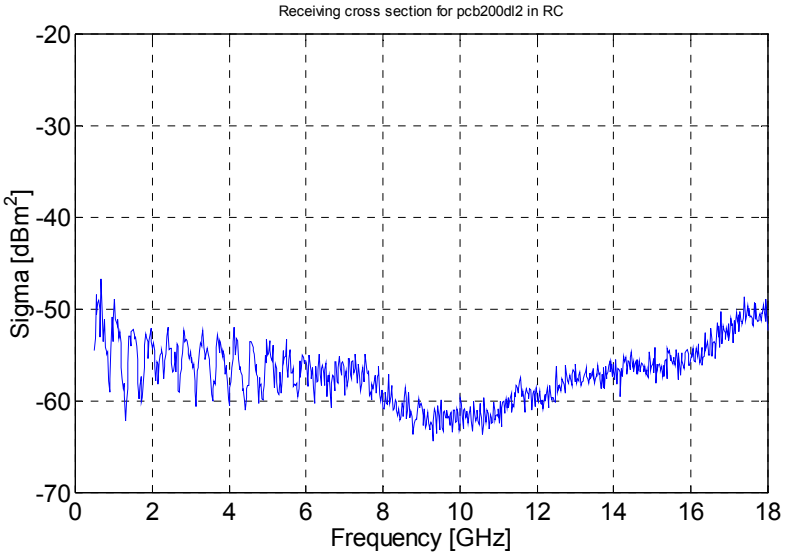

Fig. 11. Receiving cross section σ_w for pcb200dl2.

In Fig. 12 the impedance matched antenna receiving cross section σ_w for pcb200dl2 according to Eq. (9) is shown together with the theoretical bounding curve $\lambda^2/8\pi$. Comparing Fig. 12 with Fig. 5, we see that pcb200dl2 has a much lower impedance matched antenna receiving cross section than pcb200sl1 in the range 0.5 to 4 GHz. Obviously the losses, η in Eq. (3), are high.

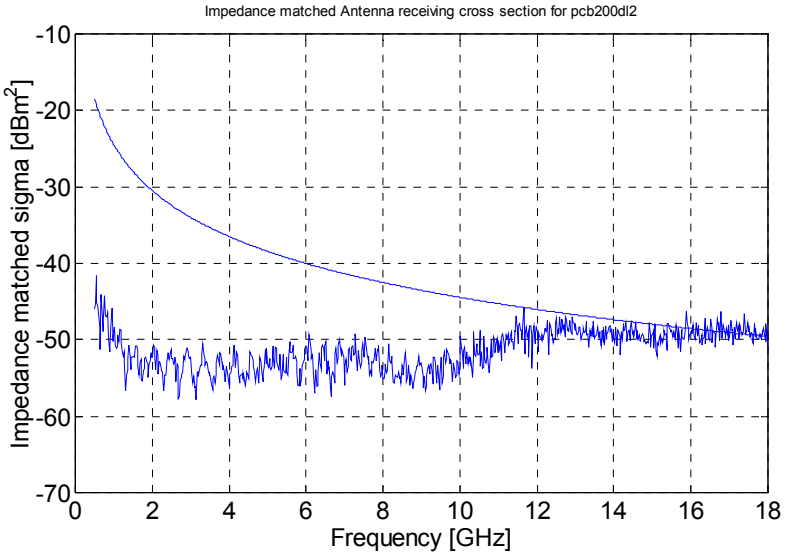

Fig. 12. Impedance matched receiving cross section for pcb200dl2 together with the bounding curve $\lambda^2/8\pi$.

In figure 13 we see the effective antenna length h_e according to Eq. (10) for pcb200dl2.
We see the influence of the input resistance R_{in} in fig. 10 on h_e, giving the peaks at approximately 5, 11, and 17 GHz.

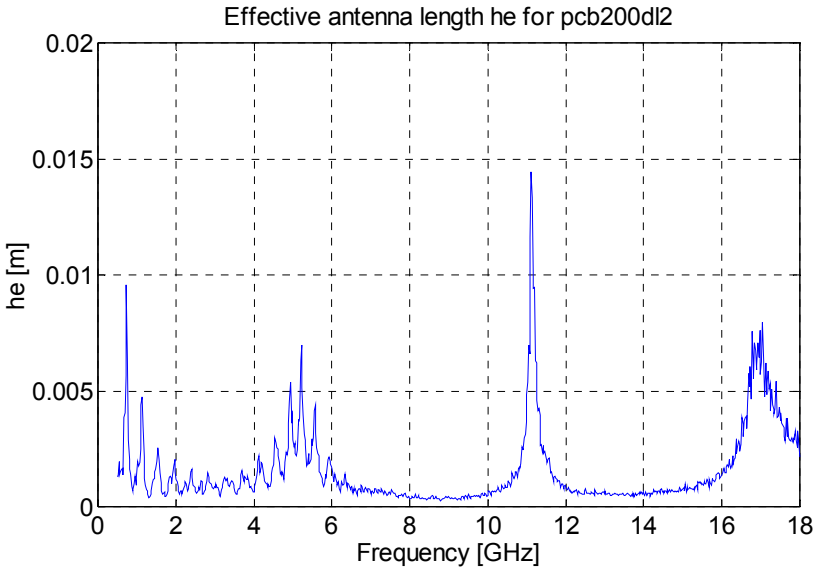

Fig. 13. Effective antenna length h_e for pcb200dl2.

In Fig. 14 the effective antenna length h_e normalized to the wavelength λ is shown. According to "EMC rules of thumb", h_e is roughly bounded by λ. In table 2 below, we present the maximum value of h_e/λ for all PCBs. All the maximum values are smaller than λ which, at least for the PCBs studied here, supports the conclusion that h_e/λ for traces on PCBs is roughly bounded by λ.

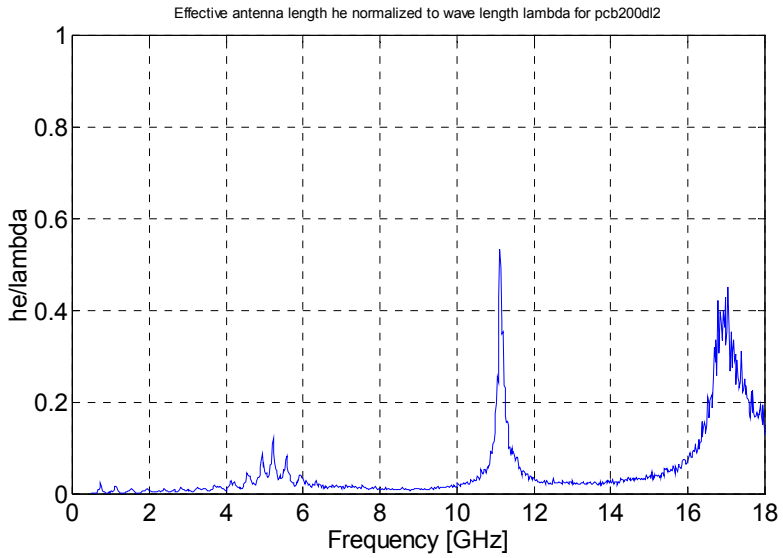

Fig. 14 The effective antenna length h_e normalized to wavelength λ for pcb200dl2.

2.3 Multi-layer PCBs

The four layer PCBs have signal traces at the top and bottom. Between the top layer and the V_{cc}-plane the core layer was 18 mil (0.457 mm) thick. Between the V_{cc}-plane and the ground plane there was a 21 mil (0.533 mm) thick layer of prepeg. Beneath the ground plane we have an 18 mil thick core layer under which the bottom signal traces were situated. The two signal traces, the ground plane and the Vcc plane are 1 oz (34 μm Cu) thick each, see Fig. 15.

On pcb100ml1 the trace length is 100 mm and the trace separation is 20 mil. The pcb200ml2 has a trace length of 200 mm and a trace separation of 50 mil. At the near end, an SMA jack is mounted between the upper signal traces. The chip resistors are according to Table 1. The cross section of the multi-layer PCBs is shown in Fig. 15. A circuit diagram for the multi-layer PCBs is given in Appendix C, page C0.

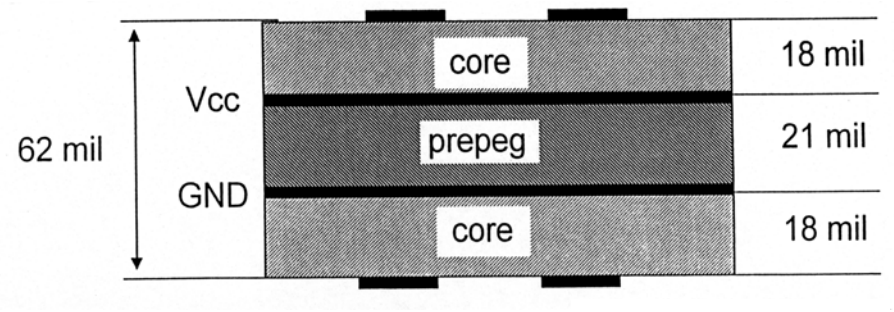

Fig 15. The cross section of the multi-layer PCBs.

Fig. 16 shows the realized gain for pcb100ml1.

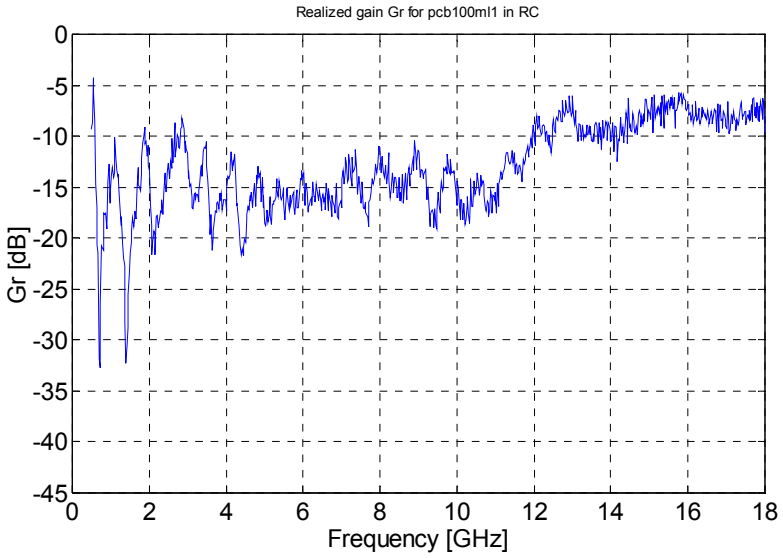

Fig. 16. Realized gain G_R for pcb100ml1.

In Fig. 17 the impedance matched receiving cross section for pcb100ml1 is plotted together with the bounding curve $\lambda^2/8\pi$. The losses according to Eq. (3) are smaller than for the double-sided PCBs (cf. Fig. 12 and Fig. 6 in Appendix C).

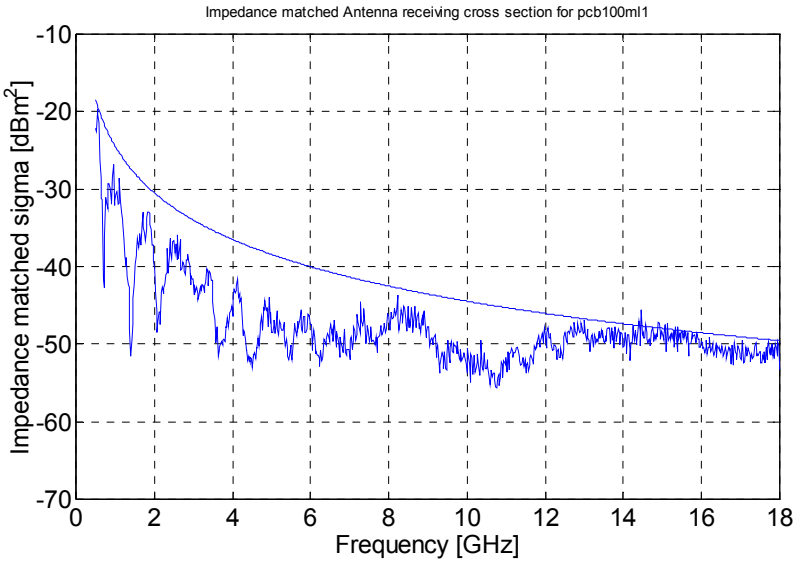

Fig. 17. Impedance matched receiving cross section for pcb100ml1 together with the bounding curve $\lambda^2/8\pi$.

In Fig. 18 we see the realized gain G_R for pcb200ml2, which is in the whole frequency range a few dB lower than for pcb100ml1, see Fig. 16.

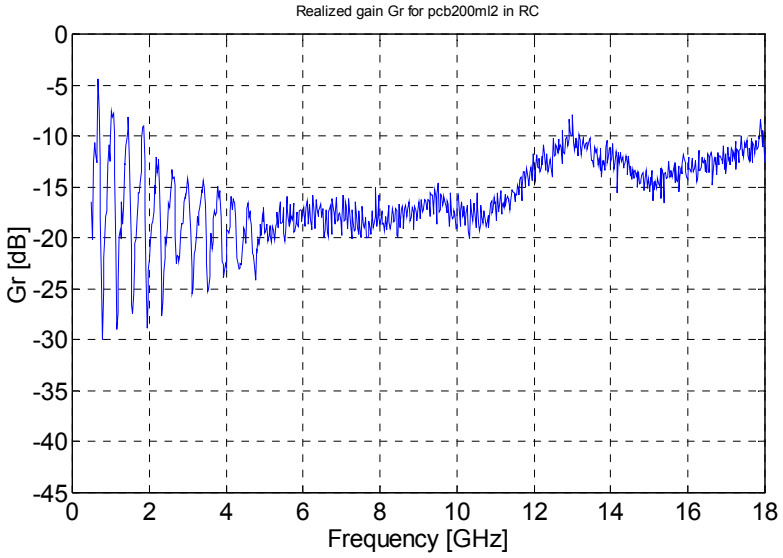

Fig. 18. Realized gain G_R for pcb200ml2.

2.4 Statistical Analysis

A comparison of the statistical distributions of coupling data of equipment measured in AC and RC [14], showed that the coupling to probes mounted inside shielded equipment measured in RC followed a χ^2-distribution with two degrees of freedom, while the coupling to equipment measured in AC did not. Our recent study of microwave field-to-wire coupling to basic wire antennas above a ground plane [1, 2] showed that the coupling measured in RC also followed a χ^2-distribution with two degrees of freedom while the coupling measured in AC did not. In order to investigate if the same conclusion could be drawn for microwave coupling to the traces on PCBs, the variance of G_R for the cases studied in this paper were plotted. Fig. 19 shows an example of such a plot for pcb200dl2.

An often used criterion for a properly working chamber is that a rectangular component of the electric field (E_R) follows a normal distribution, and thus that the power received by an antenna follows a χ^2 (chi-square) distribution with two degrees of freedom (DOF), denoted χ_2^2, at each frequency [13]. Since the variance of the normalized χ_2^2-distribution is equal to one, we can in Fig. 19 see that the variance plot seems to support the assumption that RC-data are χ^2-distributed. There is a small systematic deviation from one at the lower frequency end due to the fact that the RC is starting to degrade towards its lower frequency limit, around 0.5 GHz. This was also seen for our field-to-wire coupling measurements, see [1, 2]. A similar deviation was also reported by [12, 14].

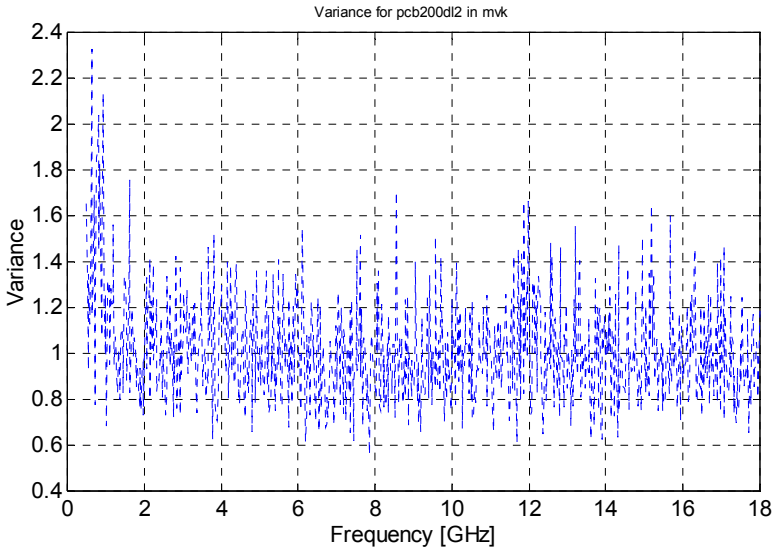

Fig. 19 Variance for pcb200dl2.

Although Fig. 19 shows that coupling data have a variance equal to 1 and thus presumably are χ^2-distributed a more exact, quantitative method, the Chi-Square Goodness-of-Fit Test [15], was used to evaluate the hypothesis that data are described by a χ_2^2-distribution. The percentage probability $\mathrm{Prob}_d(\tilde{\chi}^2 \geq \tilde{\chi}_0^2)$ of obtaining a value of $\tilde{\chi}^2 \geq \tilde{\chi}_0^2$ in an experiment with *d* degrees of freedom, as a function of d and $\tilde{\chi}_0^2$ can be calculated from the integral [16]:

$$\mathrm{Prob}_d(\tilde{\chi}^2 \geq \tilde{\chi}_0^2) = \frac{2}{2^{d/2}\Gamma(d/2)} \int_{\chi_0}^{\infty} \chi^{d-1} e^{-\chi^2/2} d\chi \qquad (12)$$

At each frequency the result is given as a probability *p*, the Rejection Significance Level, yielding the risk that one rejects the assumed distribution even if it should be correct. Normally the hypothesis is rejected if *p* is less than 5 % or 1 %.

Fig. 20 shows one example of the result of the goodness-of-fit test for the pcb200dl2, which was made for 100 stirrer positions in the RC. We see in the upper subplot that at most frequencies, except at the lower frequency end, the assumption that RC-data are χ_2^2-distributed is accepted.

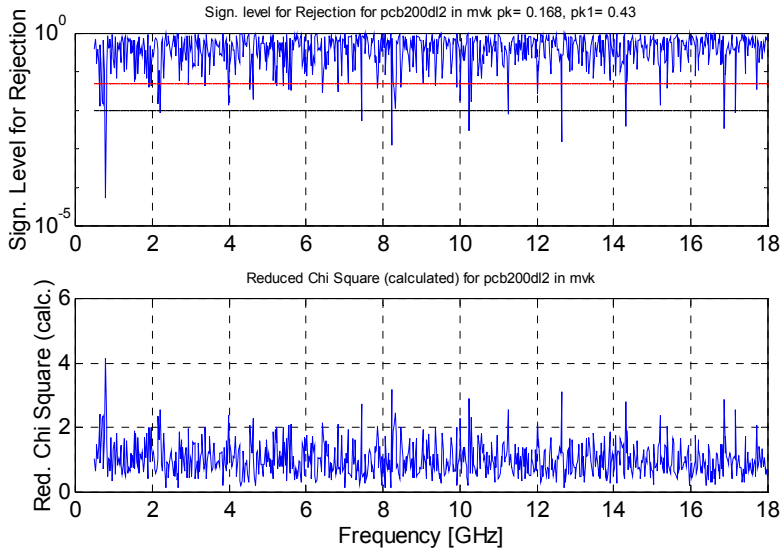

Fig. 20. Significance level for rejection (upper subplot) and the test variable "Reduced Chi Square" (lower subplot) for pcb200dl2. The test variable for the frequency range 0.5 to 18 GHz $p_k = 0.168$ and for the frequency range 1 to 18 GHz $p_{k1} = 0.43$. In the upper subplot the upper horizontal line is the 5% rejection level and the lower horizontal line is the 1% rejection level.

Since, for each PCB, the goodness-of-fit test is carried out at many frequencies, some of the *p*-values are expected to fall below e.g. the 1% level even if the expected distribution shall not be rejected. This is also seen in Fig. 20. A way to treat all data for the complete frequency range 0.5-18 GHz for each configuration is to calculate a parameter K [14, 17], according to:

$$K = -2 \cdot \sum_{i=1}^{N} \ln p_i \qquad (13)$$

where i=1 to N denotes the frequency points and p_i is the above calculated probability of rejection at each frequency. Assuming that the normalized received power is χ^2-distributed at each frequency yields that p_i is uniformly distributed. From that it can be shown that K is χ^2-distributed with 2N degrees of freedom. See Appendix G, which has been adapted from [12], for more details on the goodness-of-fit evaluation of a complete frequency interval. Thus for each value of K a corresponding probability p_k can be calculated that gives the significance level for rejecting the expected distribution for the complete frequency range.

Table 2 presents p_k for the PCBs that were studied. The results are presented as *Accepted* or *Rejected* at the 1 % significance level. From Table 2 we can see that the **RC coupling data for traces on PCBs follow a χ_2^2-distribution**. We also see that the p_k values for the RC data are generally smaller in the range 0.5 to 18 GHz than for 1 to 18 GHz. This is due to the fact that the RC is starting to degrade towards its lower frequency limit around 0.5 GHz, which is clearly seen in the variance plots. Since the statistical distribution of the power received by an antenna in the RC is known to be a χ_2^2-distribution [18], and the coupling to the traces on the PCBs, according to Table 2, also follows a χ_2^2-distribution, **we can conclude that the statistical properties of traces on PCBs are the same as those of an antenna**.

Table 2. Results of goodness-of-fit test of data from measurements in RC. Rejection if $p_k<0.01$. The expected distribution at each frequency is a χ^2_2 -distribution. The number of samples between 0.5 and 18 GHz is N=801. The fourth column presents the maximum value of the effective antenna length normalized to the wave length, Max(h_e/λ), found in the frequency range 0.5 to 18 GHz.

PCB type	**RC 0.5-18 GHz**	**RC 1-18 GHz**	**Max(h_e/λ)**
SSPCB (200SL1)	Accepted $p_k = 0.0111$	Accepted $p_k = 0.015$	0.62
SSPCB (200SL2)	Accepted $p_k = 0.15$	Accepted $p_k = 0.319$	0.74
DSPCB (100DL1)	Accepted $p_k = 0.0671$	Accepted $p_k = 0.189$	0.66
DSPCB (200DL2)	Accepted $p_k = 0.168$	Accepted $p_k = 0.430$	0.54
MLPCB (100ML1)	Rejected $p_k = 0.006$	Accepted $p_k = 0.022$	0.33
MLPCB (200ML2)	Accepted $p_k = 0.051$	Accepted $p_k = 0.13$	0.56

3 Measurement uncertainties

The FOI Reverberation chambers have been carefully investigated since a decade. The uncertainty of the measurements in the RC is determined by the statistical properties of the RC, see [7] and [19]. For the number of stirrer positions, 100 used here, we get, see Fig. 1 in [19], for all frequencies in the range 0.5 to 18 GHz an uncertainty of ± 0.8 dB for the 95 % confidence level.

4 Conclusions

For the two single-sided PCBs the trace separation for pcb200sl1 was 20 mil and for pcb200sl2 it was 50 mil. The plots of the realized gain G_R do not show any significant difference due to the different trace separation.

The two double-sided PCBs that were studied had both different trace length, 100 mm and 200 mm, and different trace separation, 20 mil and 50 mil. These differences do not qualitatively change the variation of the realized gain as a function of frequency. However, the frequency step between successive maxima of G_R , in the frequency range 0.5 to 6 GHz, is for pcb200dl2 approximately half of that for pcb100dl1. The frequency step is presumed to depend on the trace length in combination with the dielectric constant of the substrate, ε_r.

The two multi-layer PCBs had both different trace length, 100 mm and 200 mm, and different trace separation, 20 mil and 50 mil. The plots of the realized gain show some differences, but within a few dB they are in the same range. As for the double-sided PCBs, the frequency step between successive maxima of G_R, between 0.5 and 6 GHz, for pcb200ml2 is approximately half of that for pcb100ml1.

In general, double-sided and multi-layer PCBs are designed to pick up less radiation than single-sided PCBs. This can be confirmed by the present study where the realized gain of the

single-sided PCBs are generally higher (lower losses) than for the double-sided and multi-layer PCBs. Multi-layer PCBs are, due to the ground plane between the two signal layers, expected to have the smallest coupling of radiation (i.e. the lowest G_R). This study however shows that the double-sided PCBs have a lower realized gain than the others, except between 16 and 18 GHz where these G_R curves are a few dB higher than for the single-sided and multi-layer PCBs.

The impedance matched antenna receiving cross section is for all the studied PCBs bounded by the curve $\lambda^2/8\pi$, as was expected.

The effective antenna length h_e normalized to the wavelength was plotted for the different PCBs. For each PCB the maximum value of h_e/λ in the frequency interval 0.5 to 18 GHz was selected. These maxima were in the range 0.34 to 0.74. Thus we see that h_e for PCBs is bounded by λ, which was found to be the case also for our field-to-wire coupling study [1, 2].

Finally, it has been shown that microwave coupling to PCBs, measured at different stirrer positions in the RC, follows, except at the low frequency end, a χ^2-distribution with two degrees of freedom. In other words, the traces on the PCBs behave like antennas.

5 Acknowledgements

This work has been financially supported by the Supreme Commander of the Swedish Armed Forces. Stefan Silfverskiöld is also grateful for the support of the Swedish National Defence College, Stockholm. The authors would like to thank the Defense Science Organisation (DSO) in Singapore for kindly providing the PCBs that were studied.

6 References

[1] S. Silfverskiöld, M. Bäckström, J. Lorén, ”Microwave Field-to-Wire Coupling Measurements in Anechoic and Reverberation Chambers”, To be published in *IEEE Trans. on EMC, Vol. 44, Issue 1*, February 2002.

[2] S. Silfverskiöld, M. Bäckström, J. Lorén, ”Microwave Field-to-Wire Coupling Measurements in Anechoic and Reverberation Chambers*”, Scientific Report FOA-R-00-01538-612—SE*, July 2000, Swedish Defence Research Agency, Division of Sensor Technology, SE-581 11 Linköping, Sweden.

[3] M. Bäckström, J. Lorén, "Microwave Coupling into a Slotted Cavity", *Proc. of 3rd Int. Conf. on Electromagnetics in Aerospace Applications,* September 14-17, 1993, Turin, Italy.

[4] M. Bäckström, J. Lorén, "Microwave Coupling into a Slotted Cavity. Additional Results", *FOA Report FOA-R--94-00042-3.2--SE*, Sweden, December 1994.

[5] M. Bäckström, 0. Lundén, "Transmission Cross Section of Apertures Measured by Use of a Nested MSC", *Proc. of the Reverberating Chamber and Anechoic Chamber Operators Group Meeting,* December 5-7, 1995, Dahlgren, USA, pp. 211.

[6] T. Martin, M. Bäckström, J. Lorén, "Transmission Cross Section of Apertures Determined by Measurements and FDTD Simulations", *Proc. of EMC Zürich'97, Session 46H5*, February 18-20, 1997. Zürich, Switzerland, pp. 245

[7] M. Bäckström and O. Lundén, "Transmission Cross Section of Apertures Measured by Use of Nested MSC:s", *FOA-R--96-00359-3.2--SE*, December 1996, Swedish Defence Research

Agency, Division of Sensor Technology, SE-581 11 Linköping, Sweden.
[8] T. Martin and M. Bäckström, ”Semi-Empirical Modelling of Apertures by Use of FDTD”, *IEEE 1999 Int. Symp. on EMC*, pp. 832, Seattle, USA, August 2 – 6 1999.
[9] G. Göransson, ”HPM Effects on Electronic Components and the Importance of This Knowledge in Evaluation of system Susceptibility”, *IEEE 1999 Int. Symp. on EMC*, pp. 543, Seattle, USA, August 2 – 6 1999.
[10] D. A. Hill, ”Plane wave integral representation for fields in reverberation chambers”, *IEEE Trans. on EMC*, Vol. 40, No. 3, pp 209, August 1998.
[11] M. Bäckström, and J. Lorén, ”Microwave Coupling into a Generic Object.
Properties of Angular Receiving Pattern and its Significance
for Testing in Anechoic and Reverberation Chambers*”, FOI Report
FOI-R--0392--SE*, *February 2002,* Swedish Defence Research Agency, Division of Sensor Technology, SE-581 11 Linköping, Sweden.
[12] O. Lundén, M. Bäckström and N. Wellander ”Evaluation of Stirrer Efficiency in FOI Mode-Stirred Reverberation Chambers”, *FOI-R--0250--SE, November 2001*, Swedish Defence Research Agency, Division of Sensor Technology, SE-581 11 Linköping, Sweden.
[13] R.W.P. King, *”Transmission-line Theory”*, Chap. VI, Sec. 9), McGraw-Hill, New York, USA, 1955.
[14] L. Jansson and M. Bäckström, ”Directivity of Equipment and Its Effect on Testing in Mode-Stirred and Anechoic Chambers”, *IEEE 1999 Int. Symp. on EMC*, pp 17, Seattle, USA, August 2-6 1999.
[15] J. R. Taylor, *An Introduction to Error analysis,* chapter 12, 2nd ed., University Science Books, Sausalito, California, USA, 1997.
[16] E. M. Pugh and G. H. Winslow, ”The Analysis of Physical Measurements”, Addison-Wesley, Reading, Massachusetts, 1996, Section 12-8.
[17] R. B. D’Agostino and M. A. Stephens, *”Goodness-of-Fit Techniques”,* pp. 357, Marcel Dekker, Inc., New York, 1986.
[18] L. K. Warne and K. S. H. Lee, ”Some Remarks on Antenna Response in a Reverberation Chamber”, *IEEE Trans. on EMC, Vol 43, No 2*, pp. 239-240, May 2001.
[19] O. Lundén and M. Bäckström, ”Measurement of Stirrer Efficiency in Mode-Stirred Reverberation Chambers”, Technical Report *FOA-R—99-0139-612—SE*, May 1999, Swedish Defence Research Agency, Division of Sensor Technology, SE-581 11 Linköping, Sweden.

Microwave Field-to-Printed-Circuit-Board Measurements in Reverberation Chamber

Appendices

The appendices A to G contain all the results from this study of microwave field-to-printed-circuit-board coupling measurements in Reverberation Chamber (RC) made at FOI, Linköping, Sweden.

Some typical results have been presented in the text of this report.

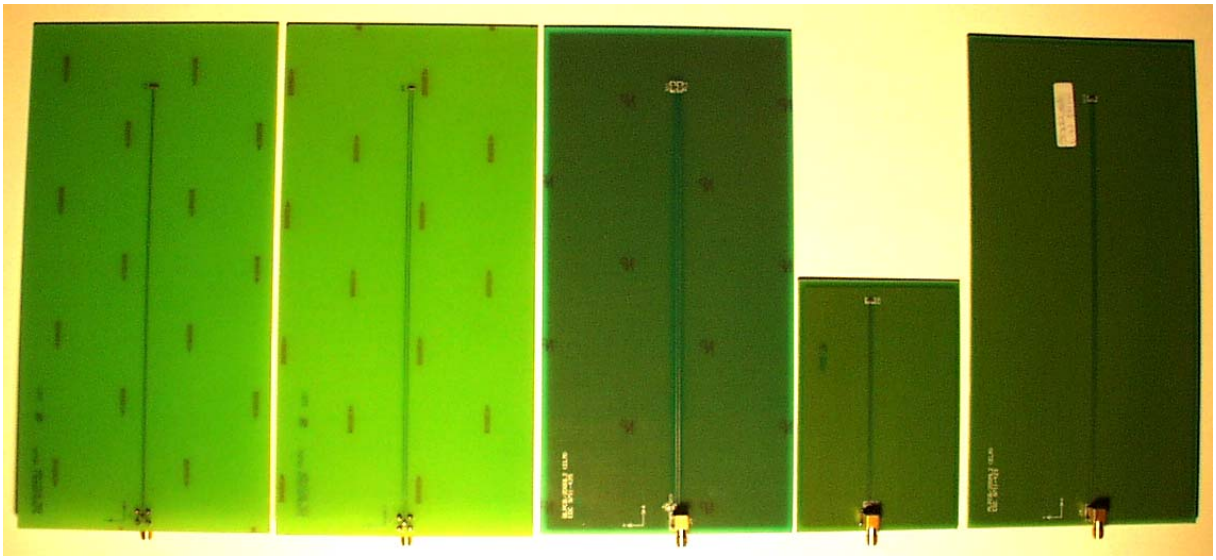

Microwave Field-to-Printed-Circuit-Board Measurements in Reverberation Chamber

Appendix A
Single-sided PCB

Fig. Circuit diagram of the single-sided PCBs.

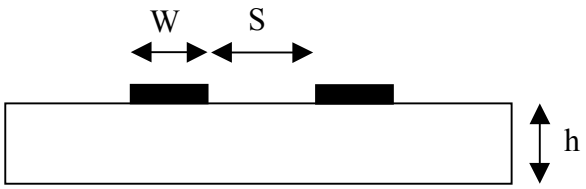

Fig. Cross-section of the single-sided PCBs.

Microwave Field-to-Printed-Circuit-Board Measurements in Reverberation Chamber

Appendix A
Single-sided PCB
PCB200SL1

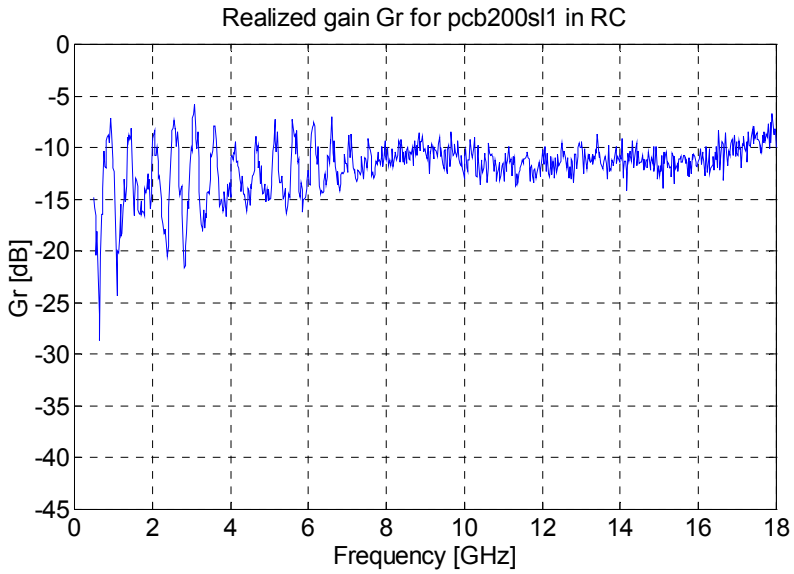

Fig. 1. G_R for pcb200sl1

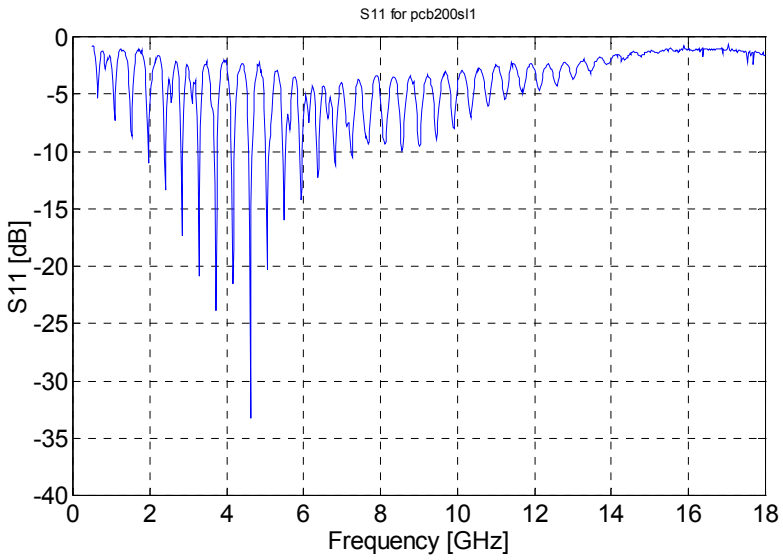

Fig. 2. S_{11} for pcb200sl1

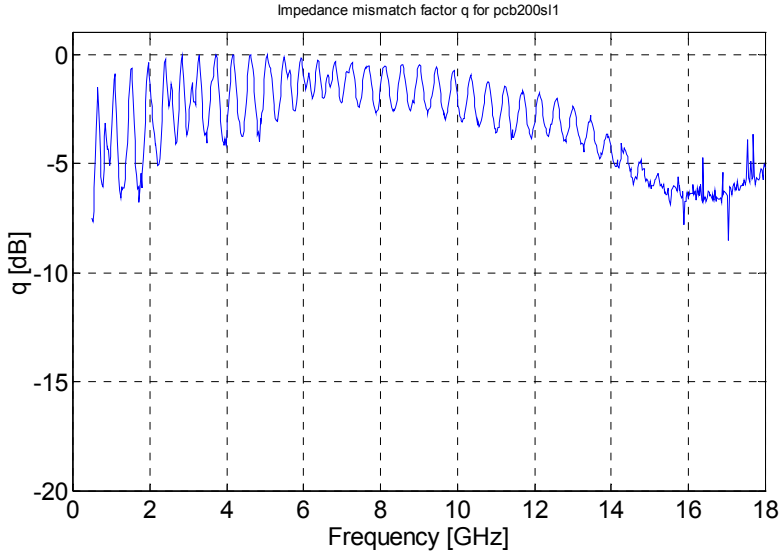

Fig. 3. Impedance mismatch factor q for pcb200sl1

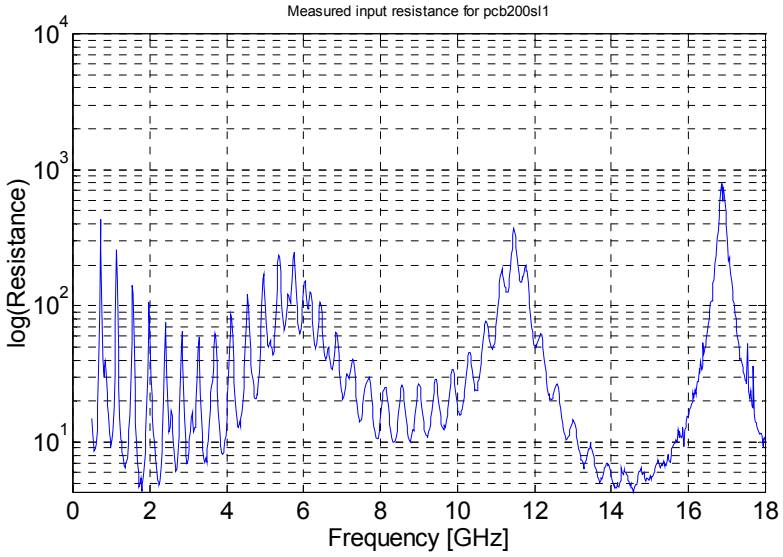

Fig. 4. Input resistance R_{in} for pcb200sl1

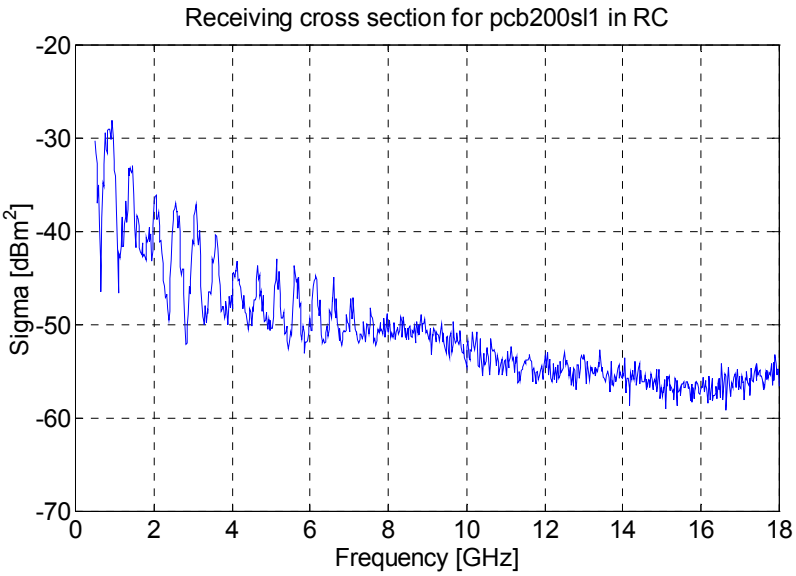

Fig. 5. Receiving cross section σ_w for pcb 200sl1

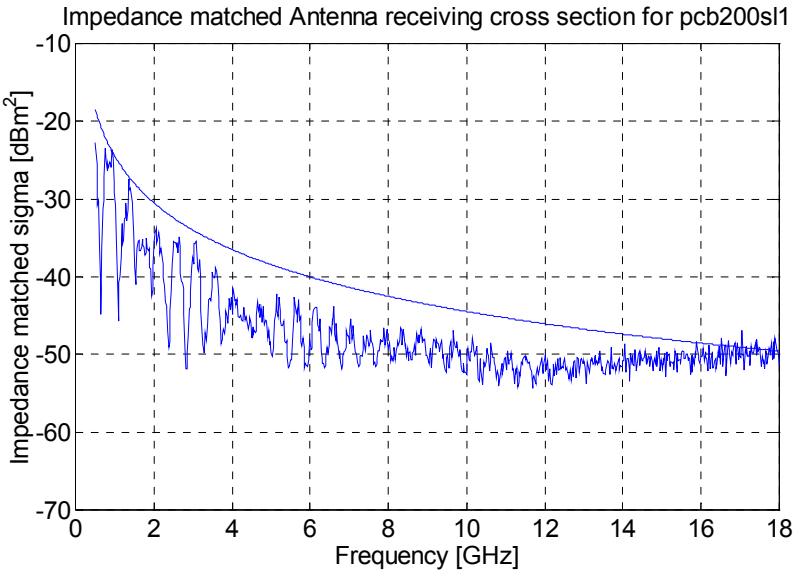

Fig. 6. Impedance matched receiving cross section for pcb200sl1

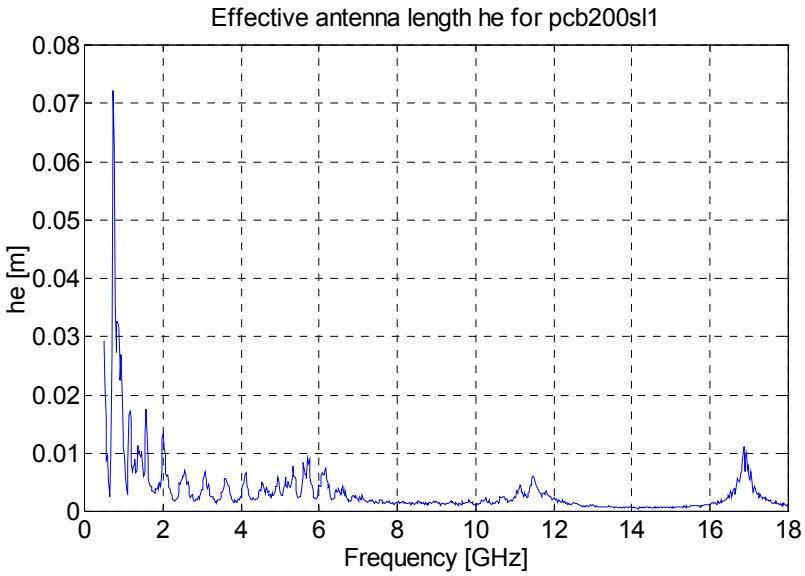

Fig. 7. Effective antenna length h_e for pcb200sl1

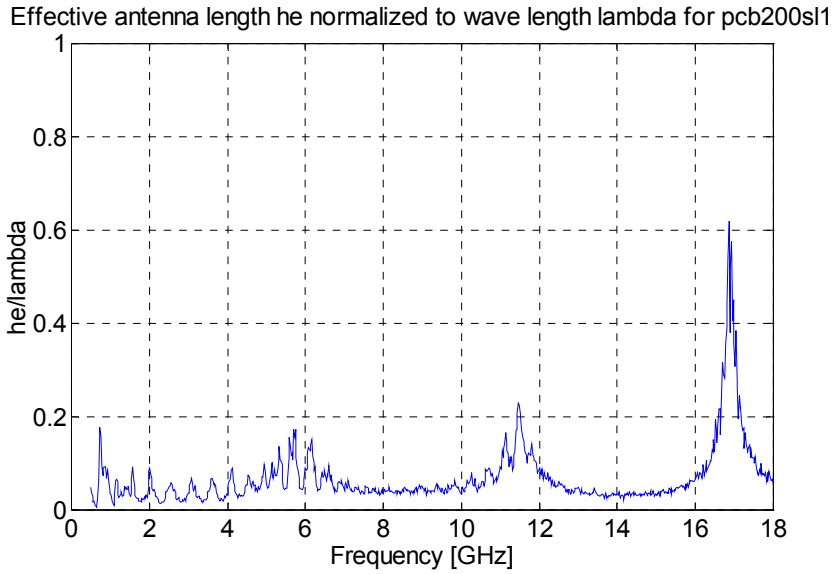

Fig. 8. Effective antenna length normalized to wavelength λ

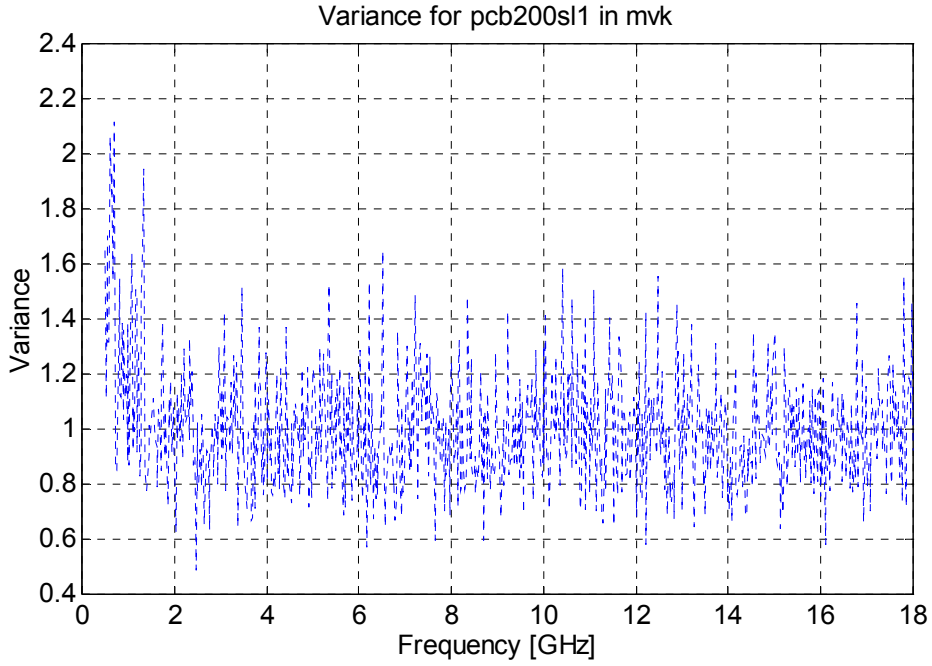

Fig. 9. Variance for pcb200sl1

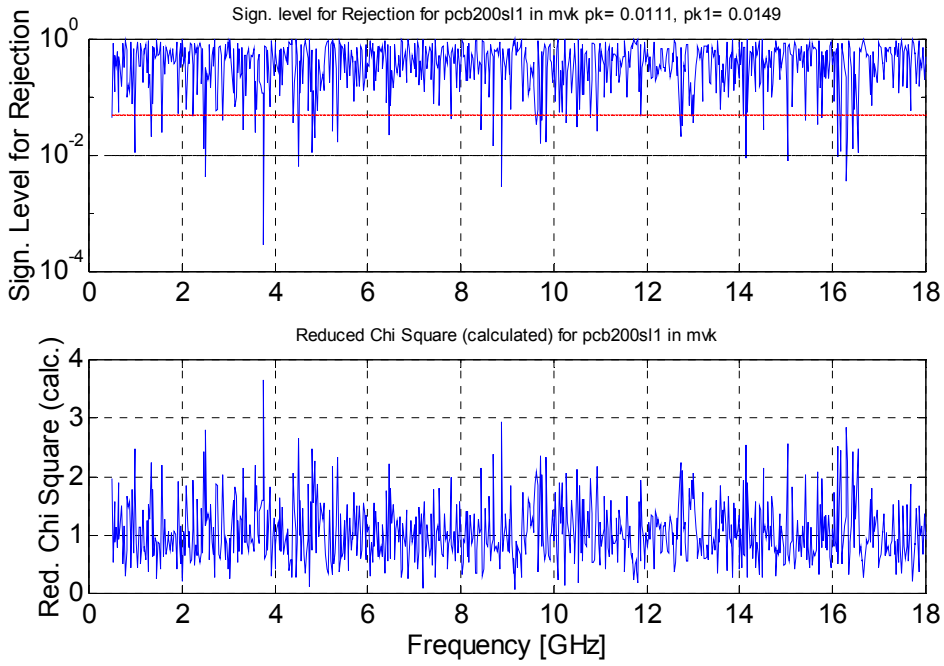

Fig. 10. Significance level for rejection (upper subplot) and the test variable ”Reduced Chi Square” (lower subplot) for pcb200sl1. p_k=0.0111, p_{k1}=0.0149

Microwave Field-to-Printed-Circuit-Board Measurements in Reverberation Chamber

Appendix B
Single-sided PCB
PCB200SL2

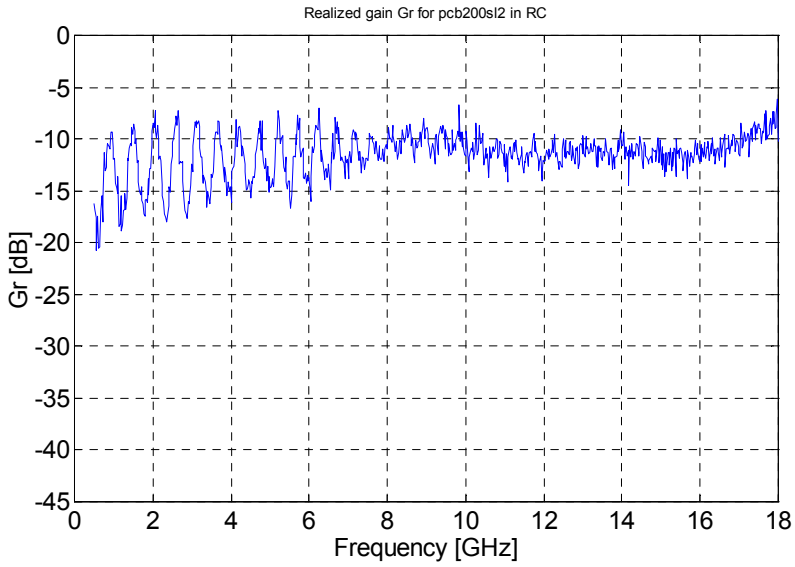

Fig. 1. G_R for pcb200sl2

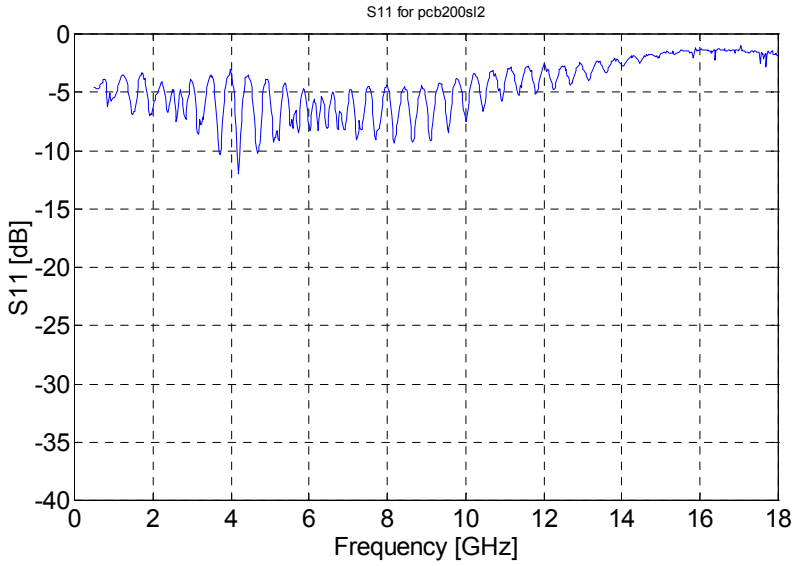

Fig. 2. S_{11} for pcb200sl2

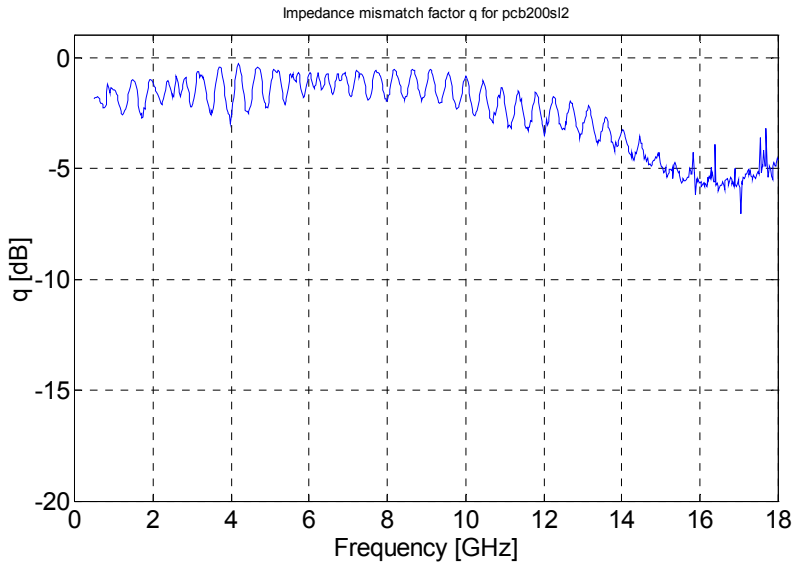

Fig. 3. Impedance mismatch factor q for pcb200sl2

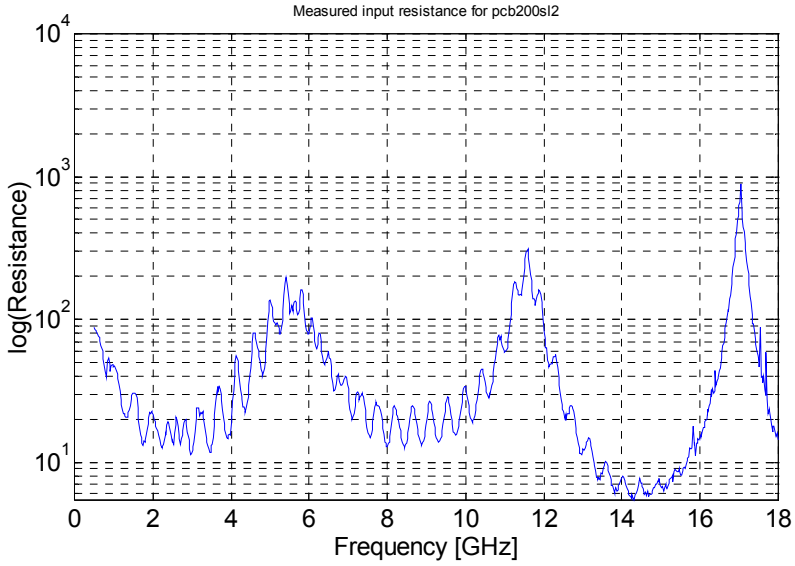

Fig. 4. Input resistance R_{in} for pcb200sl2

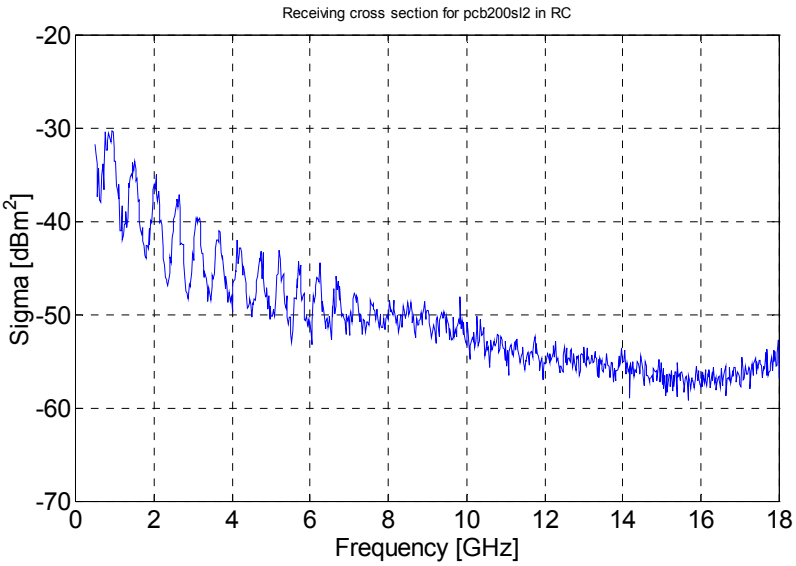

Fig. 5. Receiving cross section σ_w for pcb200sl2

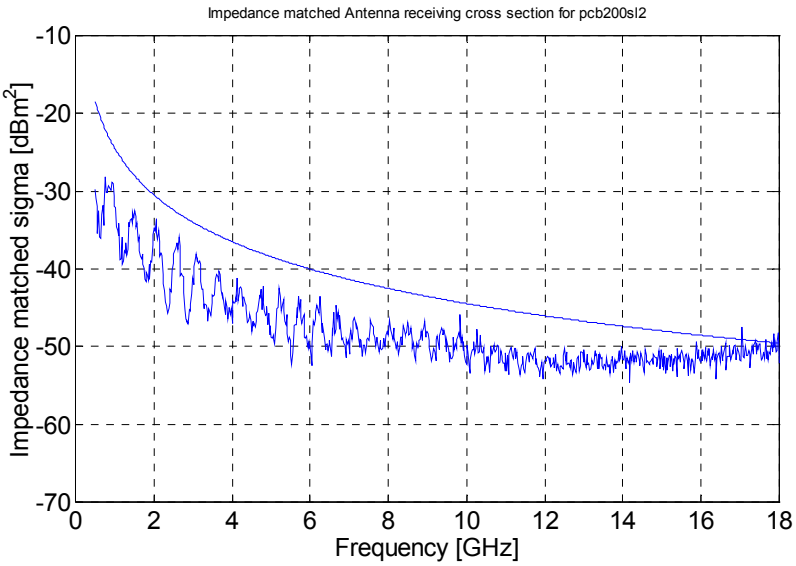

Fig. 6. Impedance matched receiving cross section for pcb200sl2

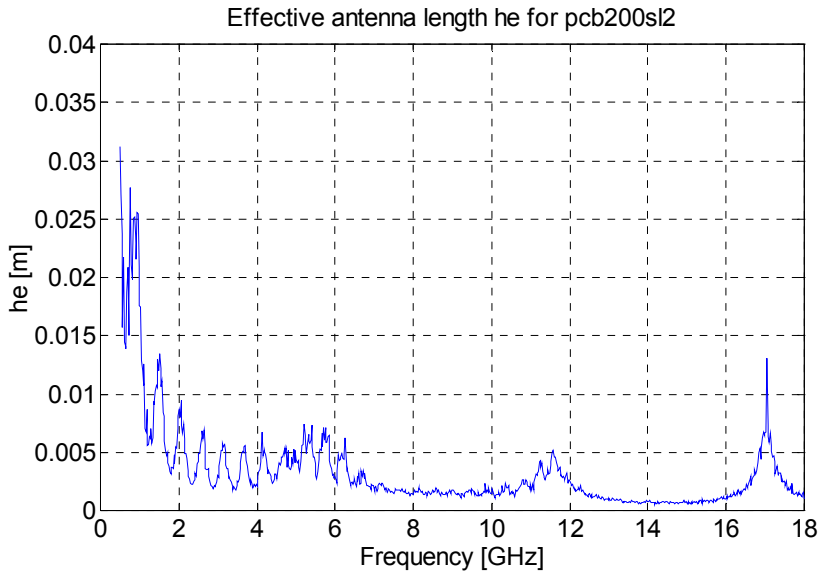

Fig. 7. Effective antenna length h_e for pcb200sl2

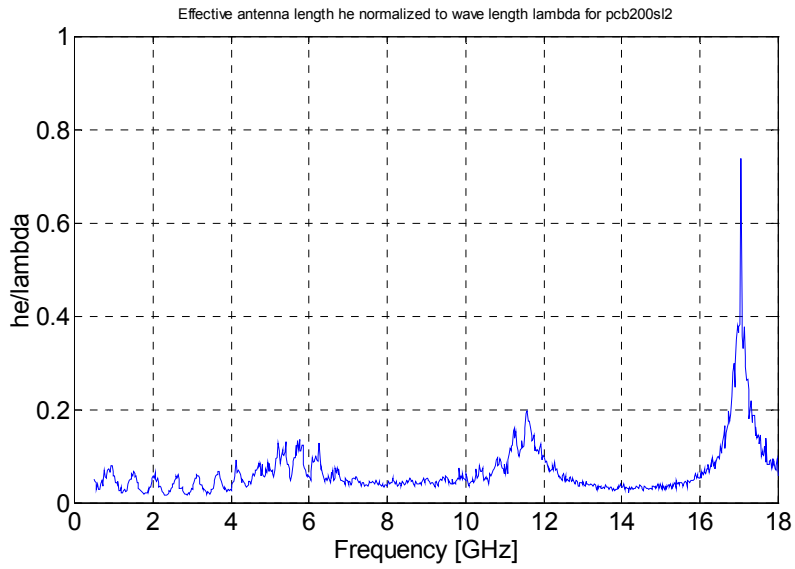

Fig. 8. Effective antenna length normalized to wavelength λ for pcb200sl2.

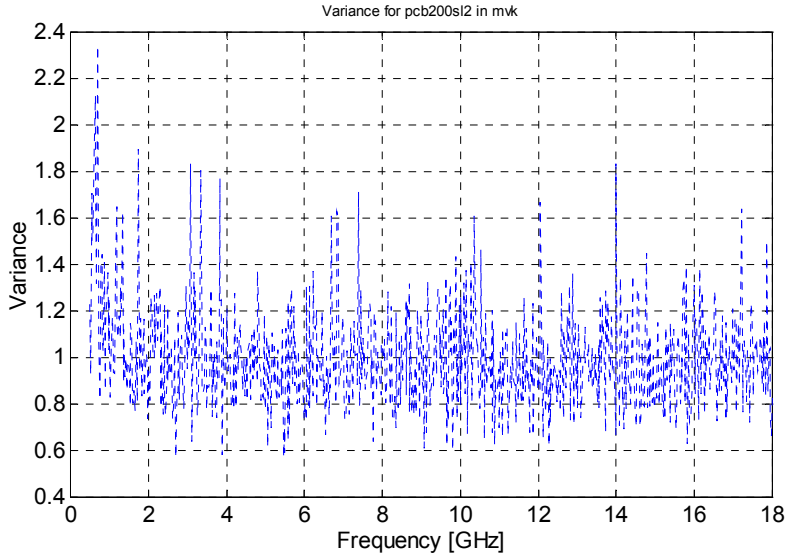

Fig. 9. Variance for pcb200sl2.

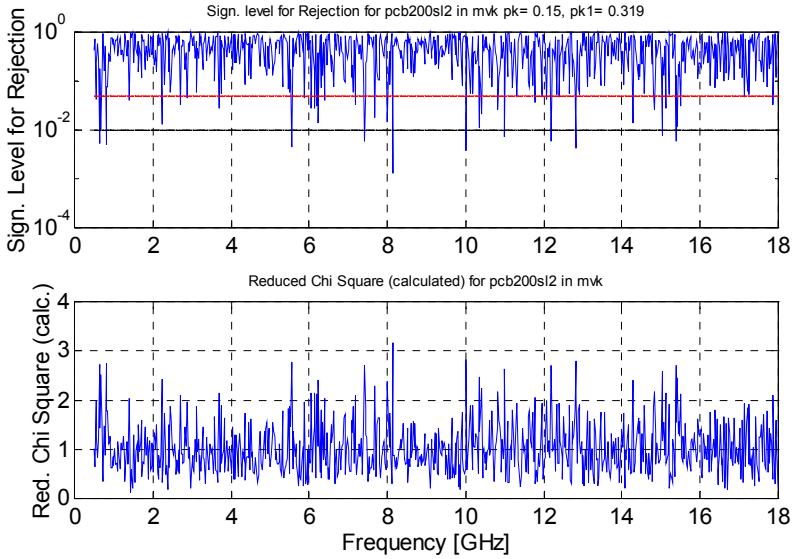

Fig. 10. Significance level for rejection (upper subplot) and the test variable ”Reduced Chi Square” (lower subplot) for pcb200sl2. p_k=0.15, p_{k1}=0.319.

Microwave Field-to-Printed-Circuit-Board Measurements in Reverberation Chamber

Appendix C
Double-sided PCB

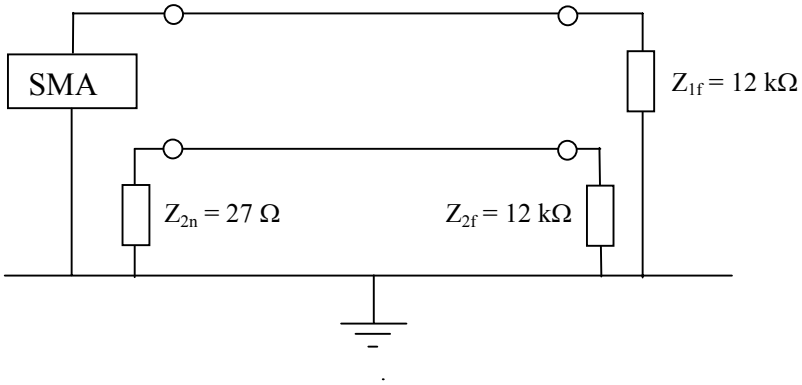

Fig. Circuit diagram of the double-sided PCBs.

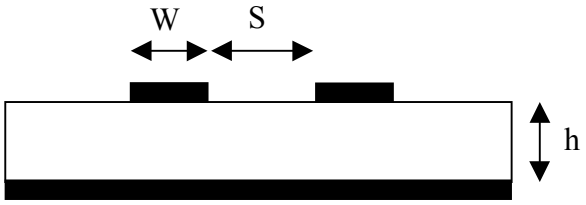

Fig. Cross-section of the double-sided PCBs.

Microwave Field-to-Printed-Circuit-Board Measurements in Reverberation Chamber

Appendix C
Double-sided PCB
PCB100DL1

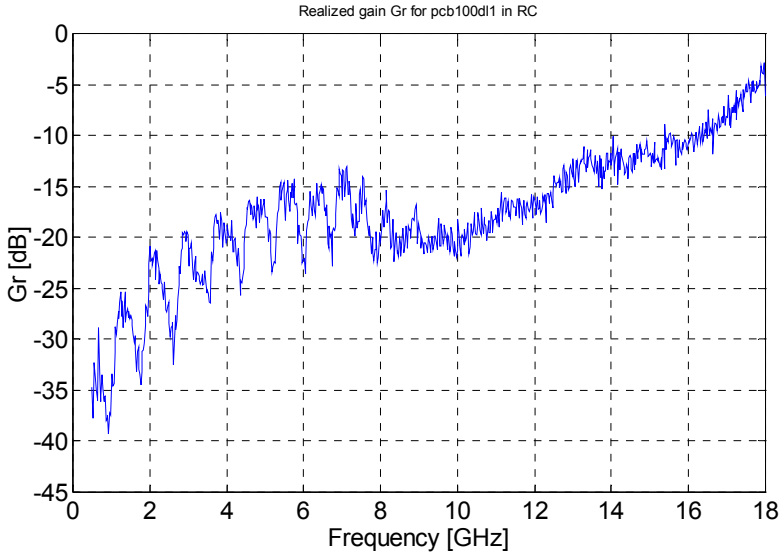

Fig. 1. G_R for pcb100dl1

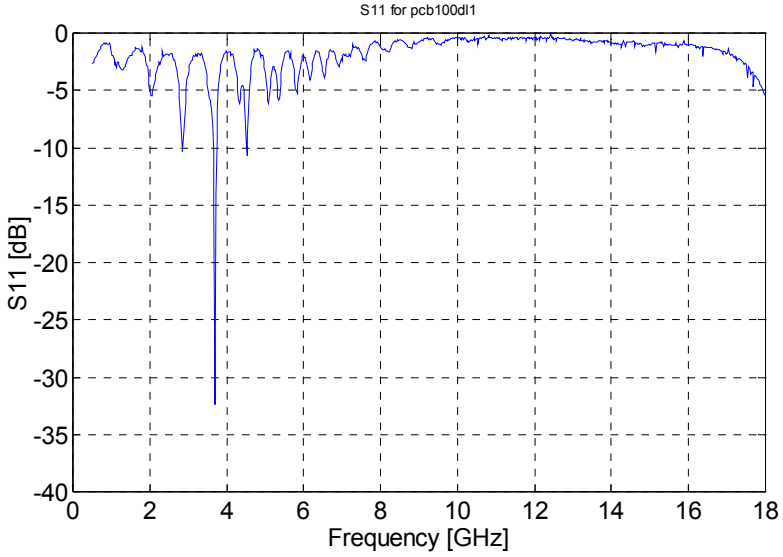

Fig. 2. S_{11} for pcb100dl1

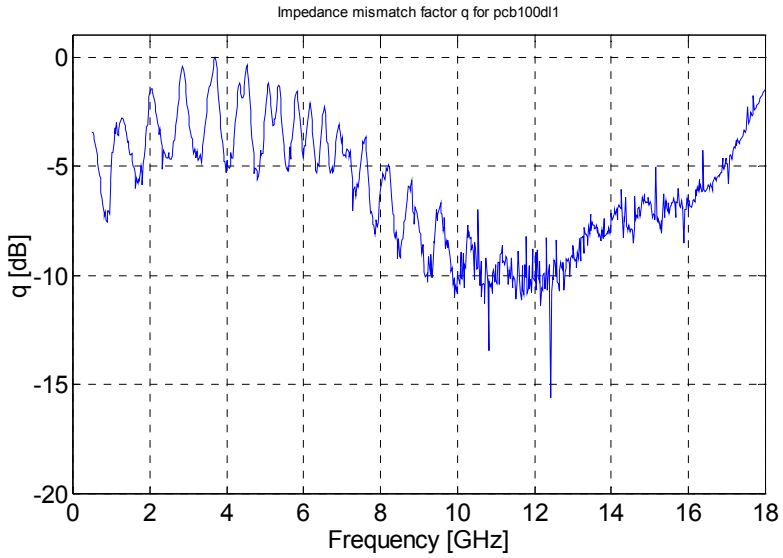

Fig. 3. Impedance mismatch factor q for pcb100dl1

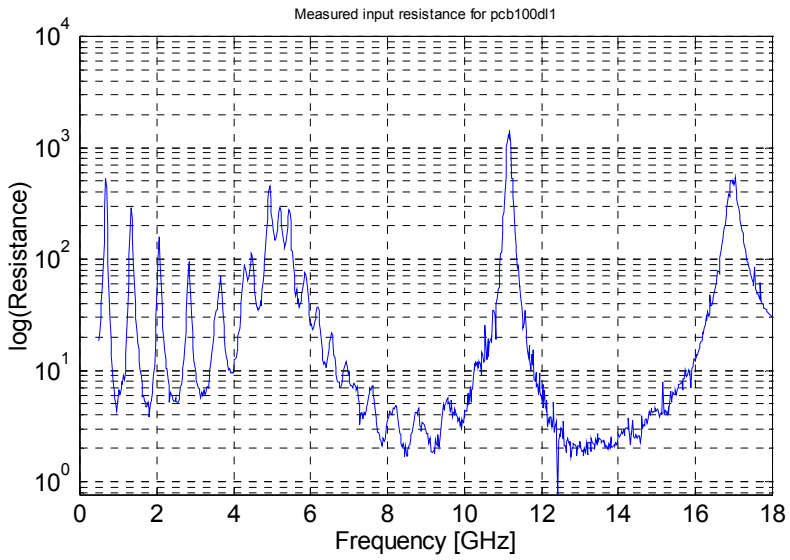

Fig. 4. Input resistance R_{in} for pcb100dl1

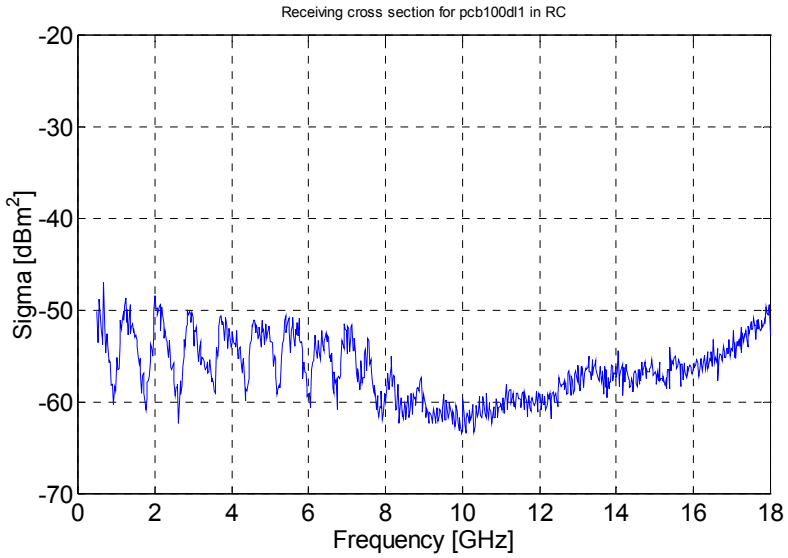

Fig. 5. Receiving cross section σ_w for pcb100dl1

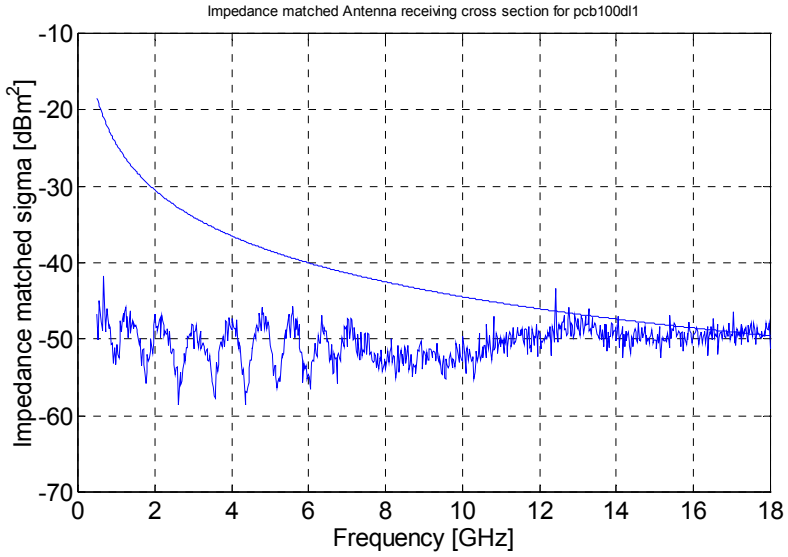

Fig. 6. Impedance matched receiving cross section for pcb100dl1

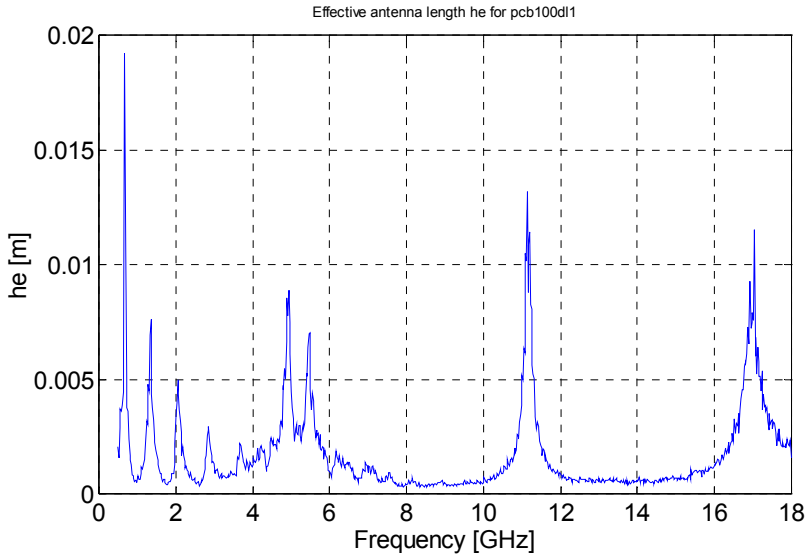

Fig. 7. Effective antenna length h_e for pcb100dl1

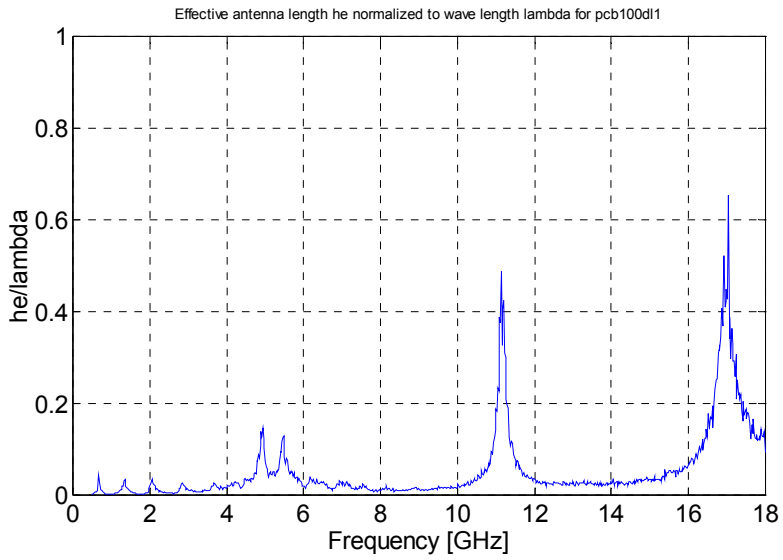

Fig. 8. Effective antenna length normalized to wavelength λ for pcb100dl1

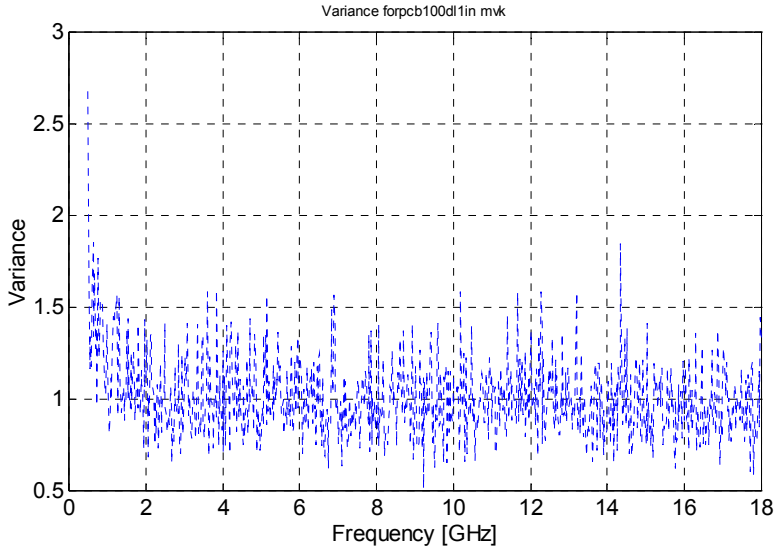

Fig. 9. Variance for pcb100dl1

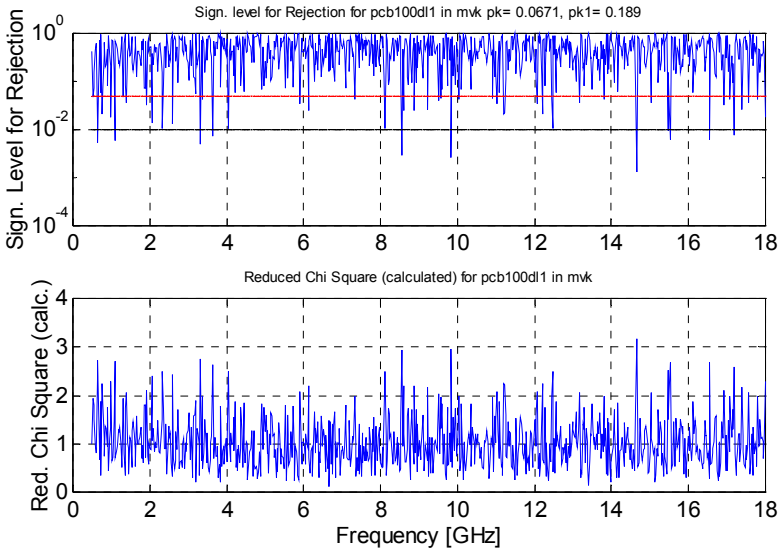

Fig. 10. Significance level for rejection (upper subplot) and the test variable ”Reduced Chi Square” (lower subplot) for pcb100dl1. p_k=0.067, p_{k1}=0.189.

Microwave Field-to-Printed-Circuit-Board Measurements in Reverberation Chamber

Appendix D
Double-sided PCB
PCB200DL2

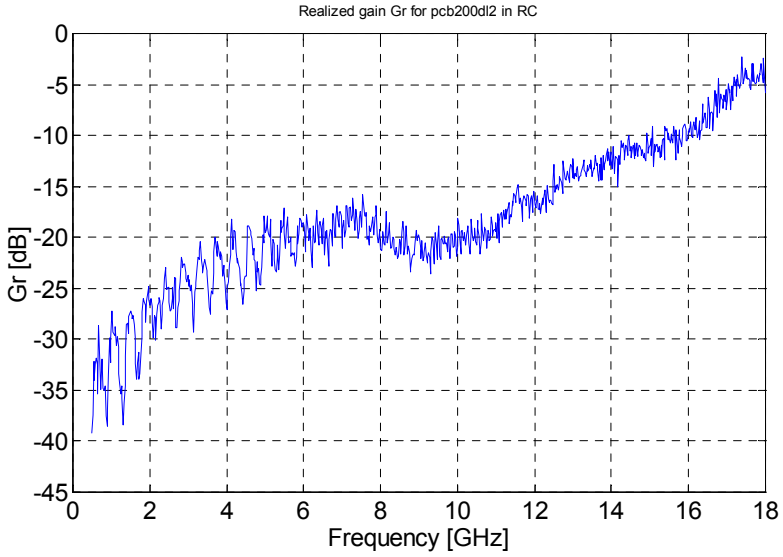

Fig. 1. G_R for pcb200dl2

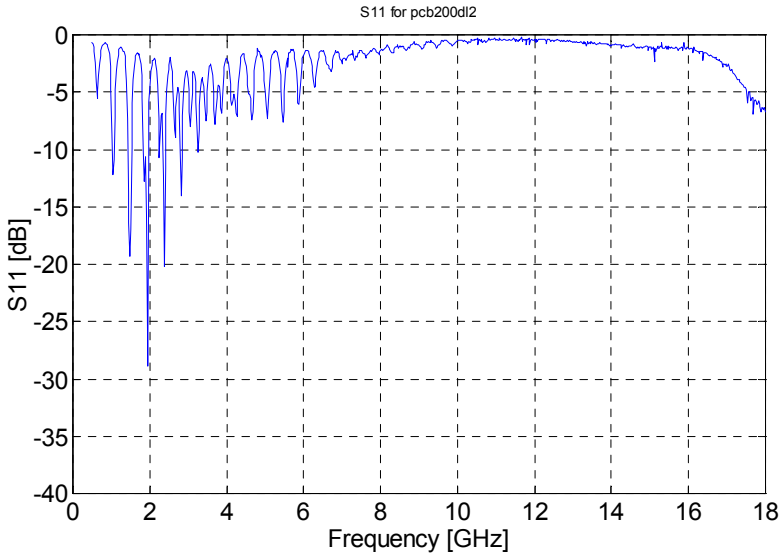

Fig. 2. S_{11} for pcb200dl2

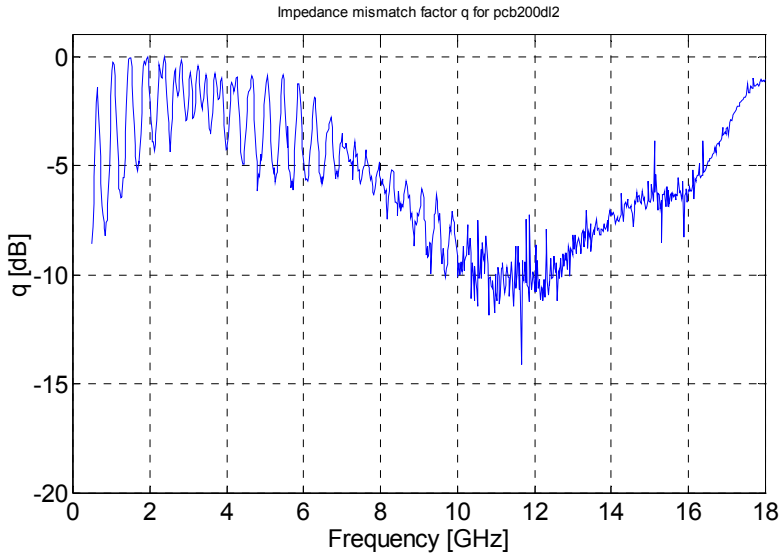

Fig. 3. Impedance mismatch factor q for pcb200dl2

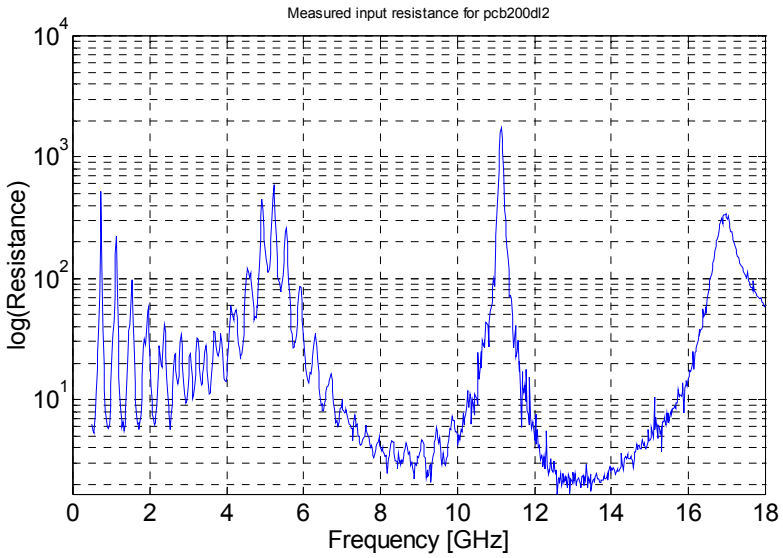

Fig. 4. Input resistance R_{in} for pcb200dl2

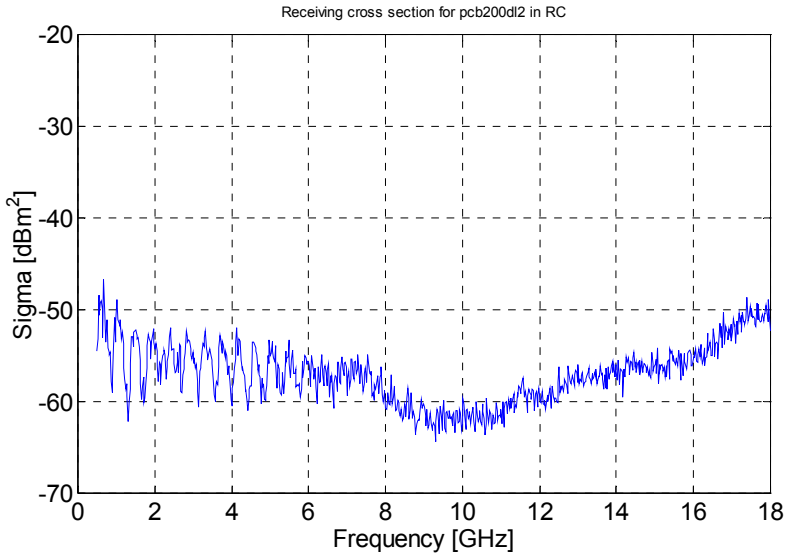

Fig. 5. Receiving cross section σ_w for pcb200dl2

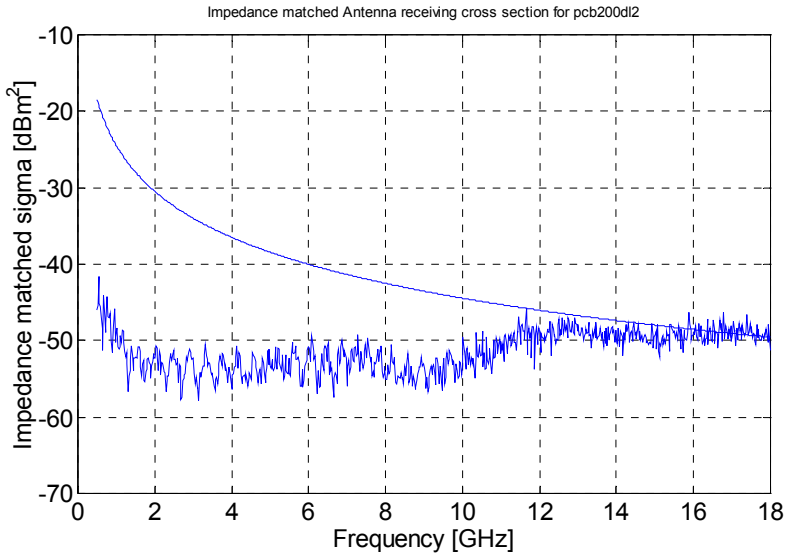

Fig. 6. Impedance matched receiving cross section for pcb200dl2

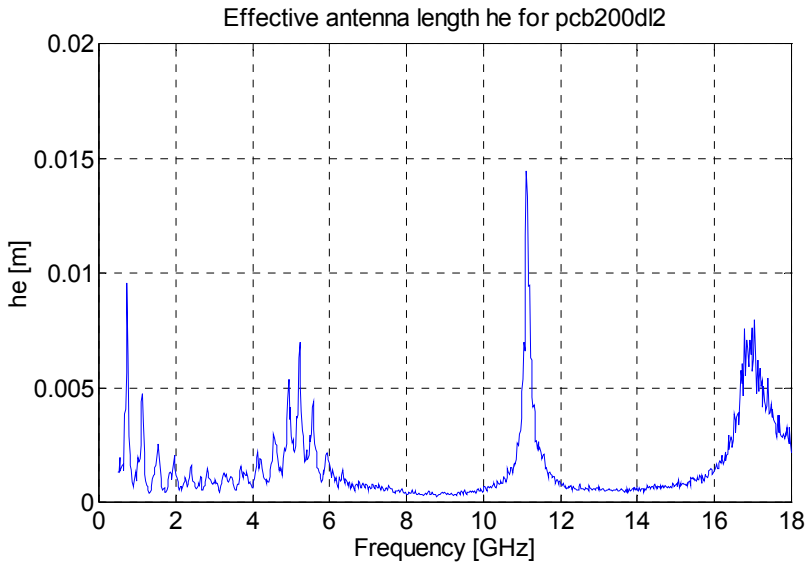

Fig. 7. Effective antenna length h_e for pcb200dl2

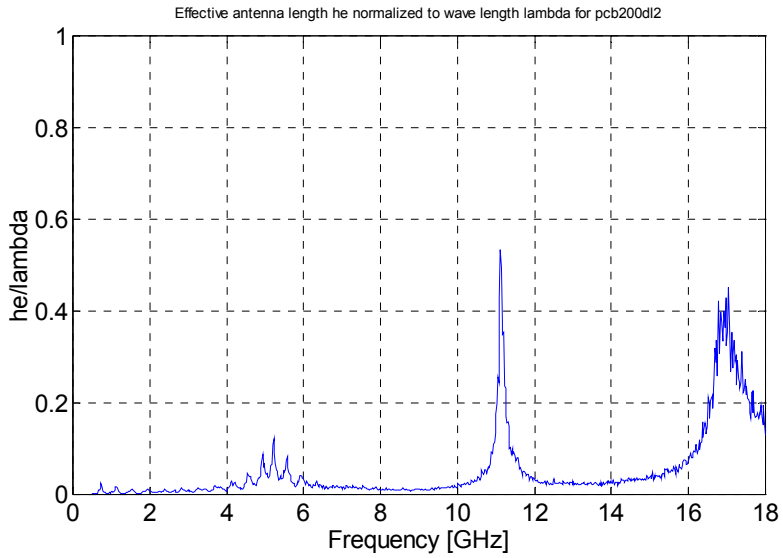

Fig. 8. Effective antenna length normalized to wavelength λ for pcb200dl2.

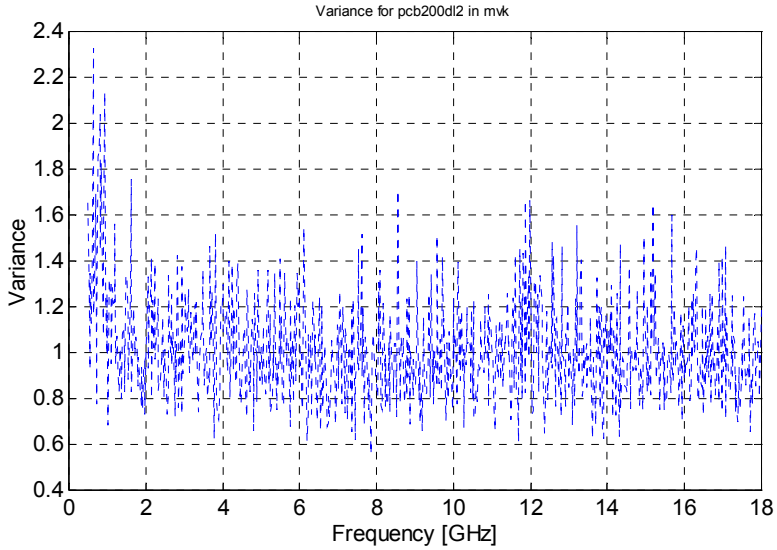

Fig. 9. Variance for pcb200dl2

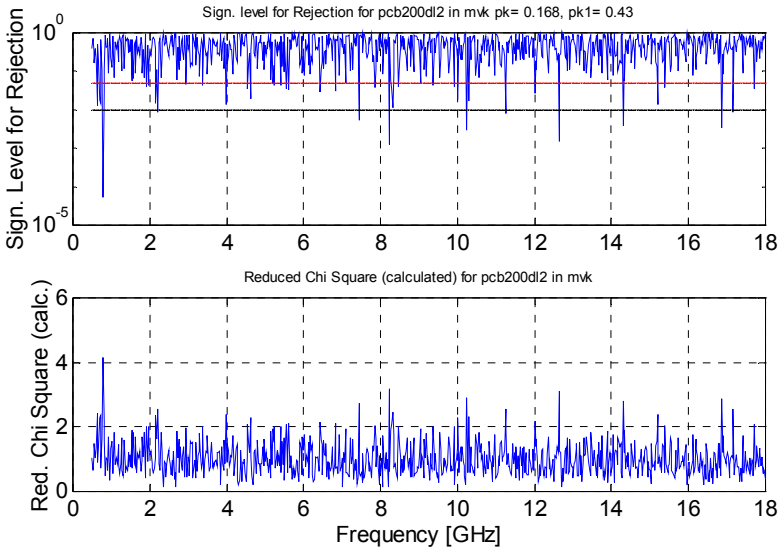

Fig. 10. Significance level for rejection (upper subplot) and the test variable ”Reduced Chi Square” (lower subplot) for pcb200dl2. p_k=0.168, p_{k1}=0.43

Microwave Field-to-Printed-Circuit-Board Measurements in Reverberation Chamber

Appendix E
Multi-layer PCB

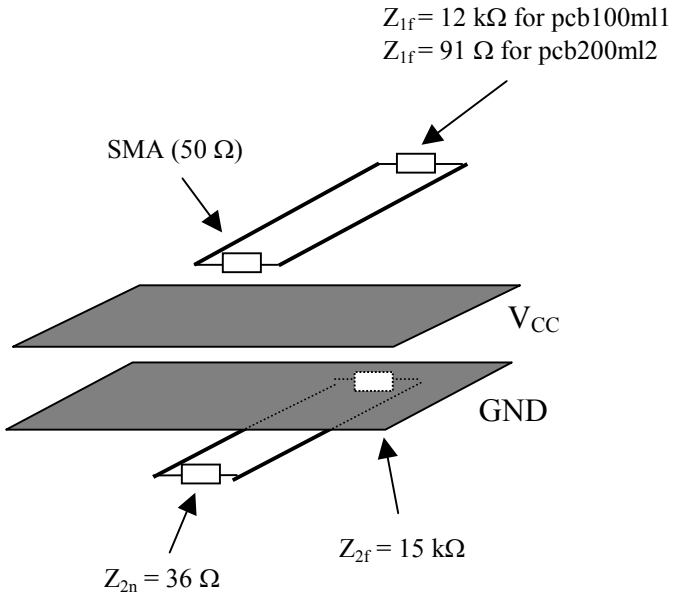

Fig. Circuit diagram of the multi-layer PCBs.

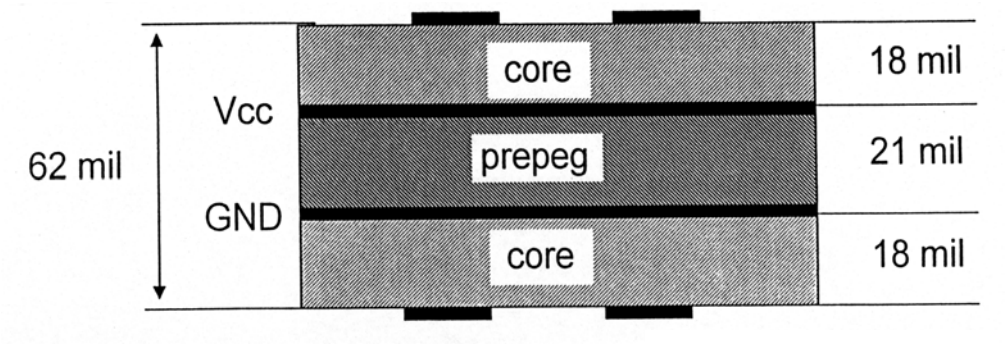

Fig. Cross-section of the multi-layer PCBs

Microwave Field-to-Printed-Circuit-Board Measurements in Reverberation Chamber

Appendix E
Multi-layer PCB
PCB100ML1

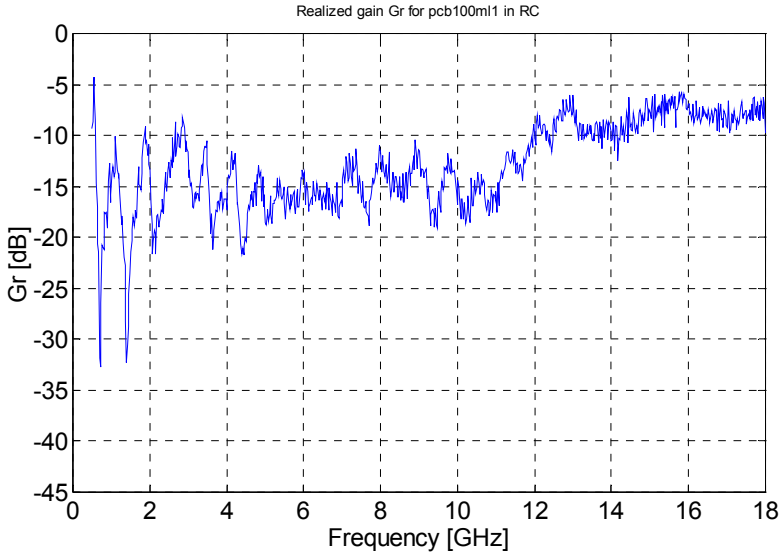

Fig. 1. G_R for pcb100ml1

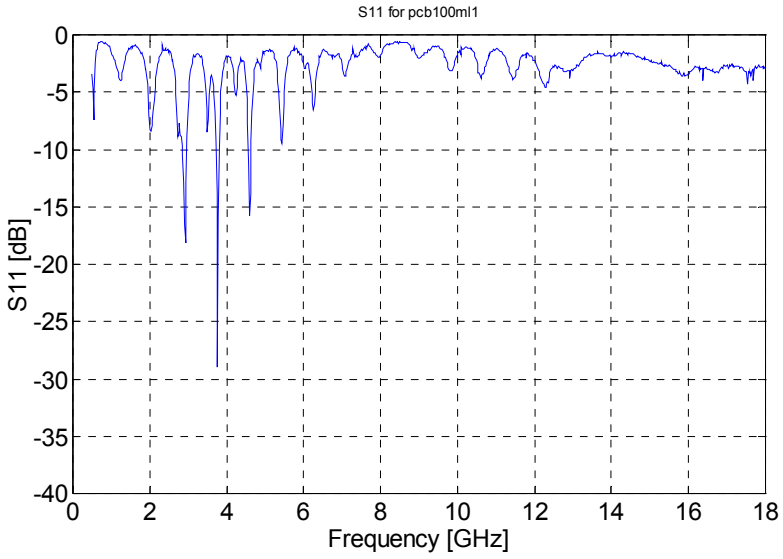

Fig. 2. S_{11} for pcb100ml1

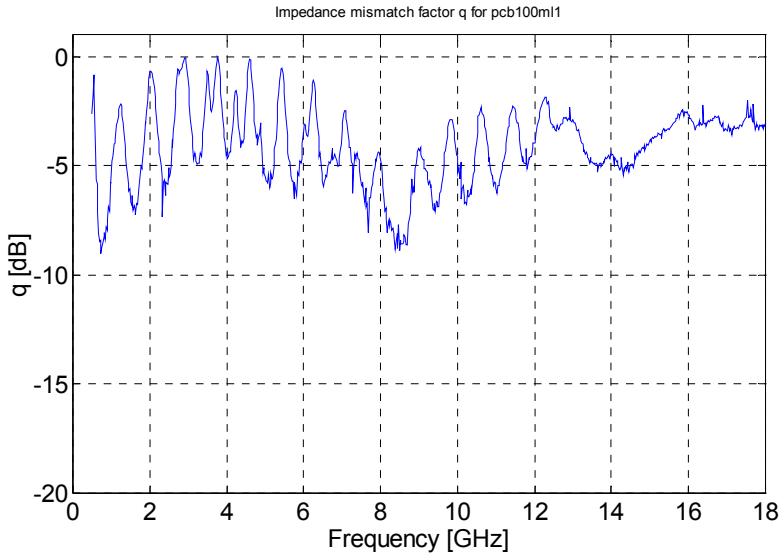

Fig. 3. Impedance mismatch factor q for pcb100ml1

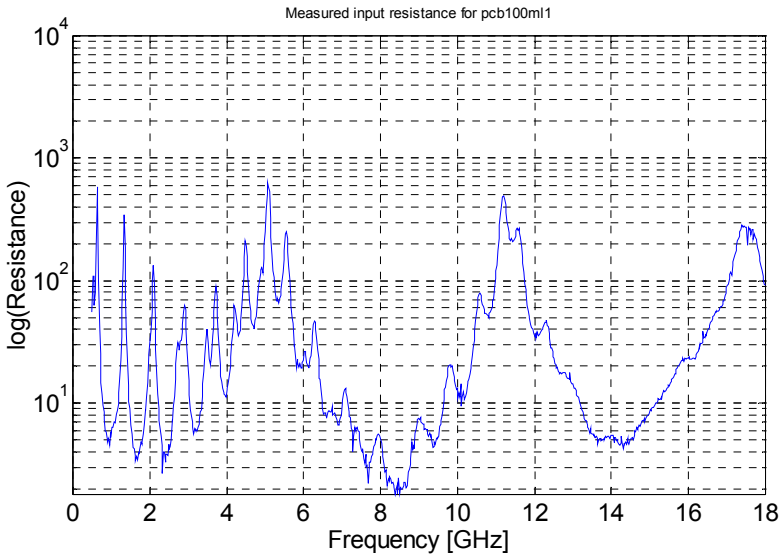

Fig. 4. Input resistance R_{in} for pcb100ml1

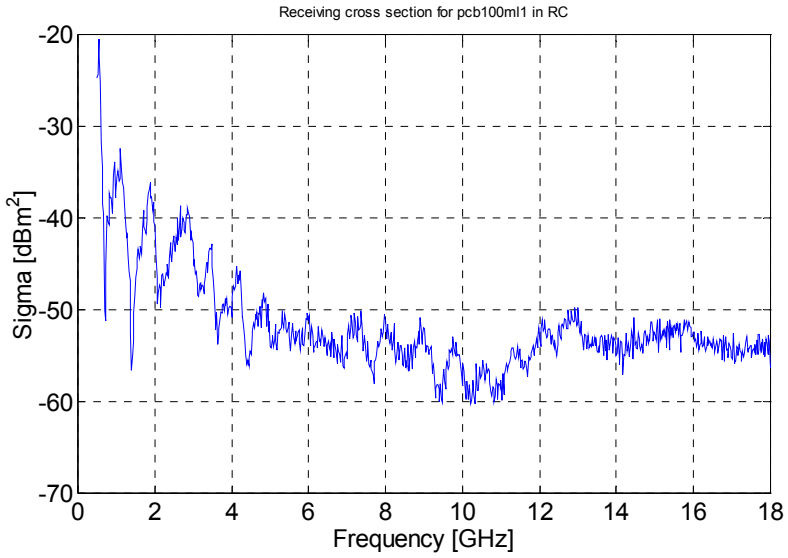

Fig. 5. Receiving cross section σ_w for pcb100ml1

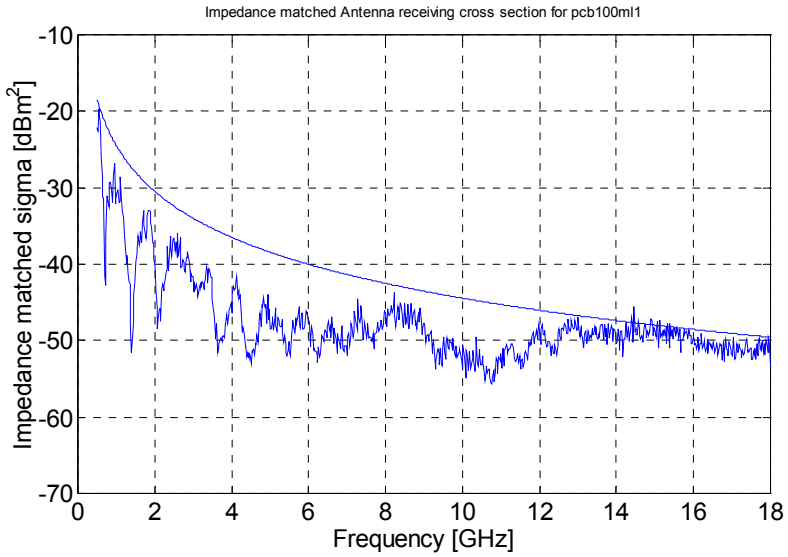

Fig. 6. Impedance matched receiving cross section for pcb100ml1

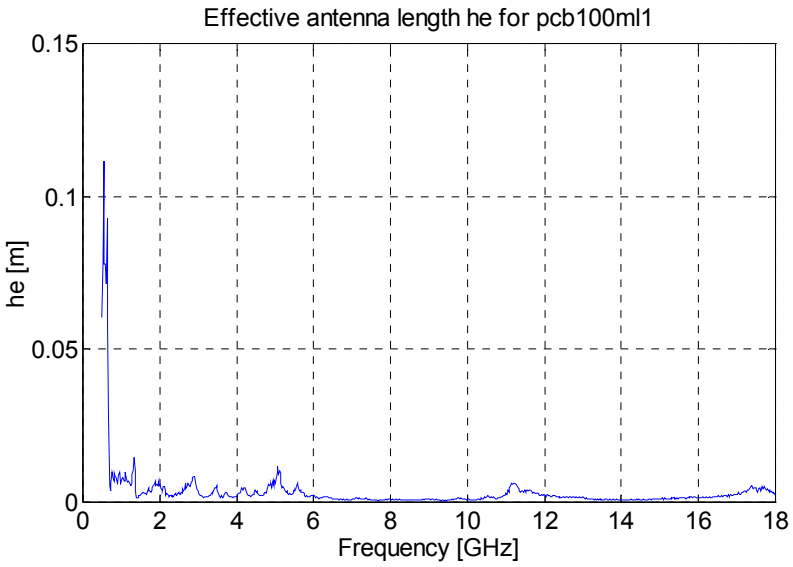

Fig. 7. Effective antenna length h_e for pcb100ml1

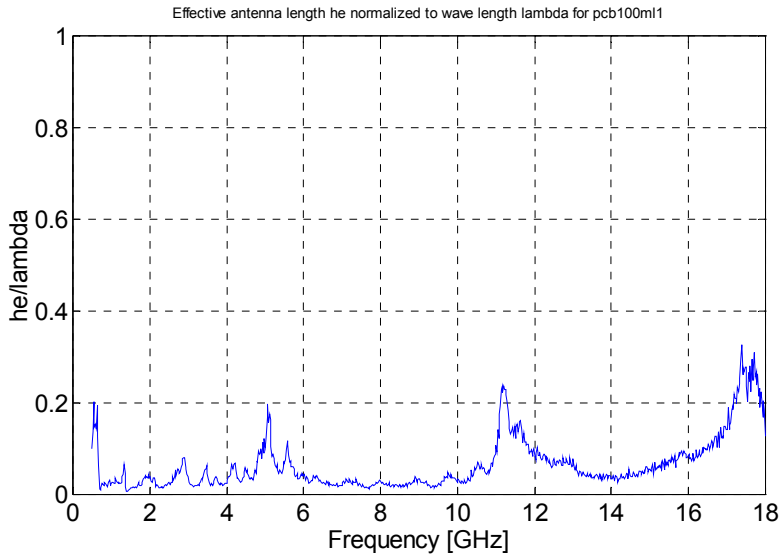

Fig. 8. Effective antenna length normalized to wavelength λ for pcb100ml1.

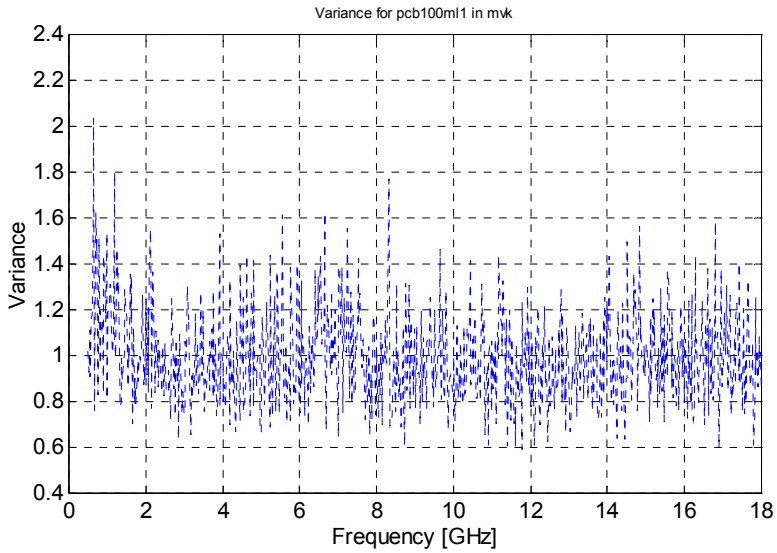

Fig. 9. Variance for pcb100ml1.

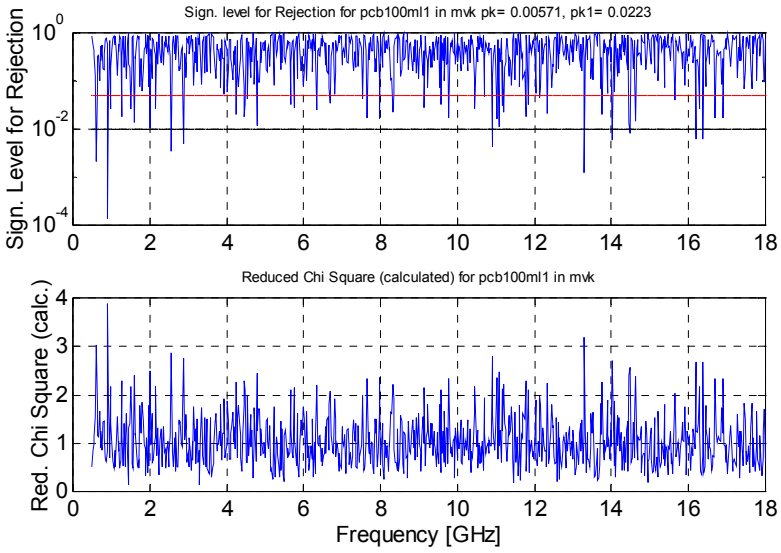

Fig. 10. Significance level for rejection (upper subplot) and the test variable ”Reduced Chi Square” (lower subplot) for pcb100ml1. p_k=0.0571, p_{k1}=0.0223.

Microwave Field-to-Printed-Circuit-Board Measurements in Reverberation Chamber

Appendix F
Multi-layer PCB
PCB200ML2

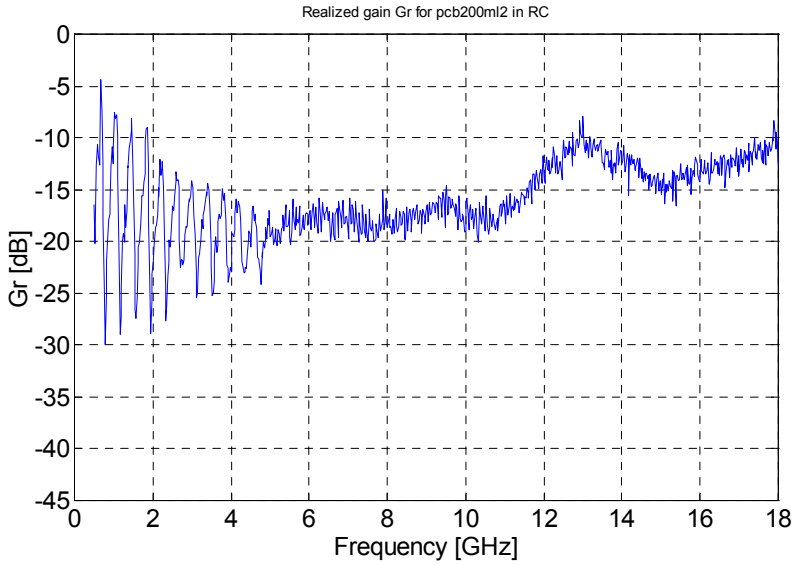

Fig. 1. G_R for pcb200ml2

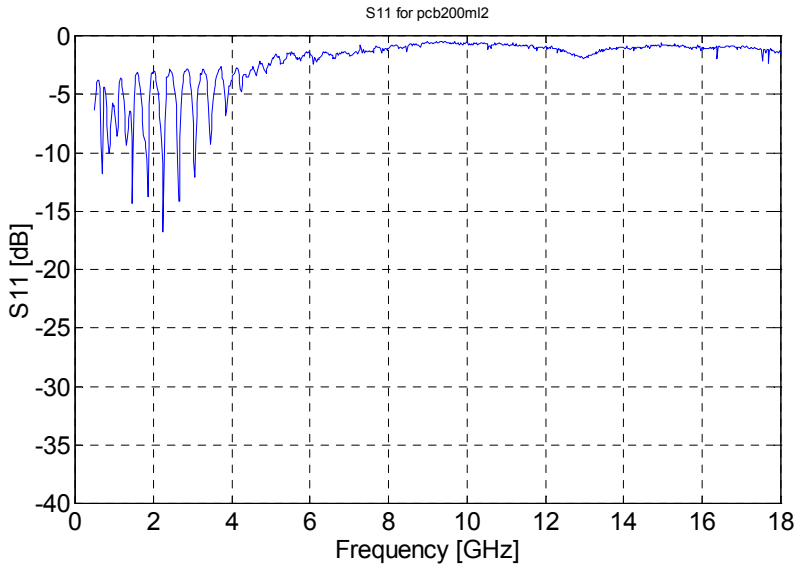

Fig. 2. S_{11} for pcb200ml2

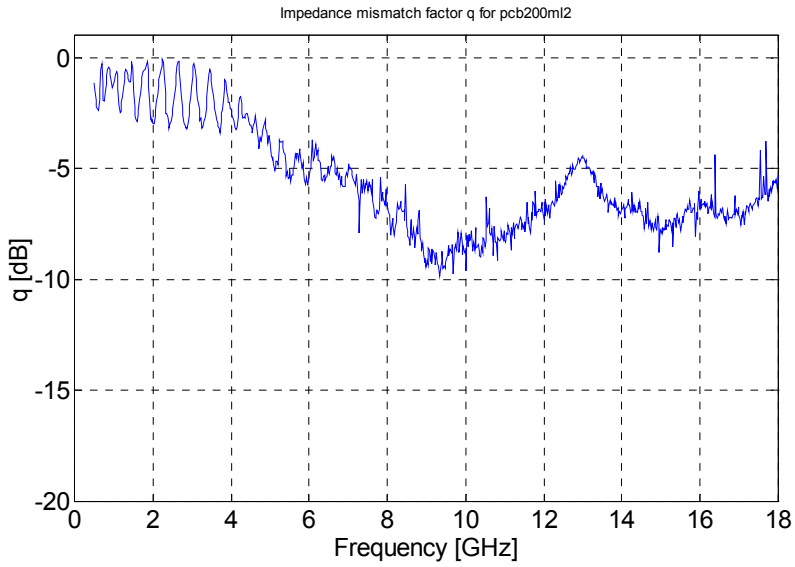

Fig. 3. Impedance mismatch factor q for pcb200ml2

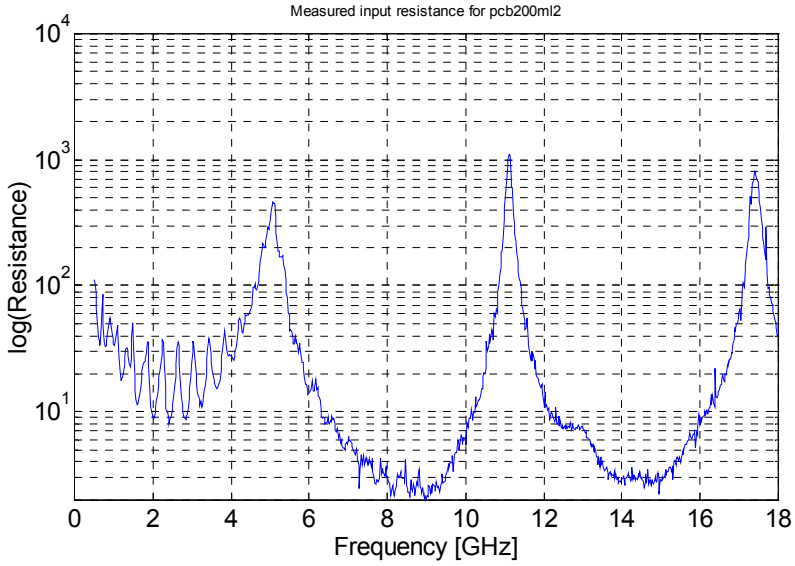

Fig. 4. Input resistance R_{in} for pcb200ml2

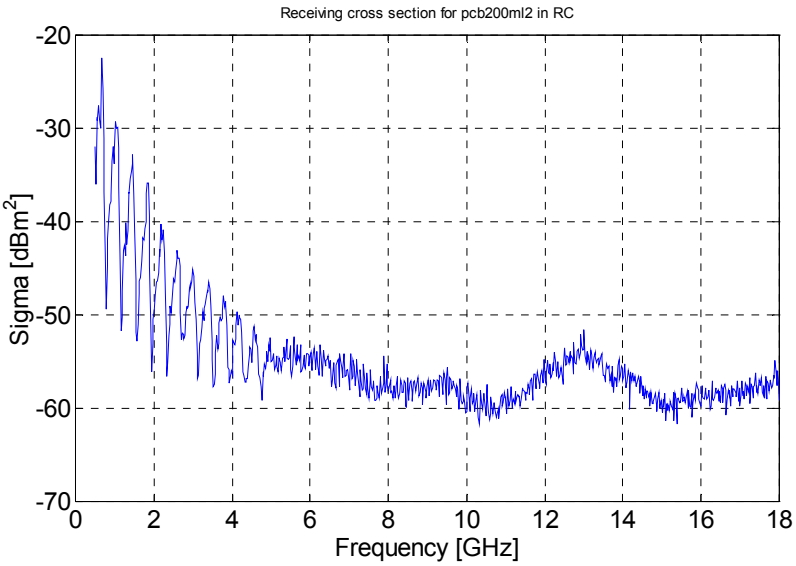

Fig. 5. Receiving cross section σ_w for pcb200ml2

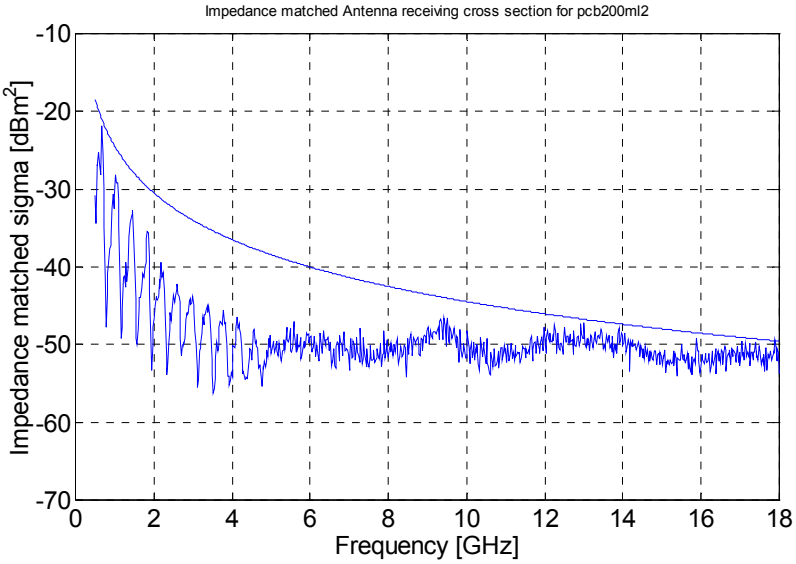

Fig. 6. Impedance matched receiving cross section for pcb200ml2

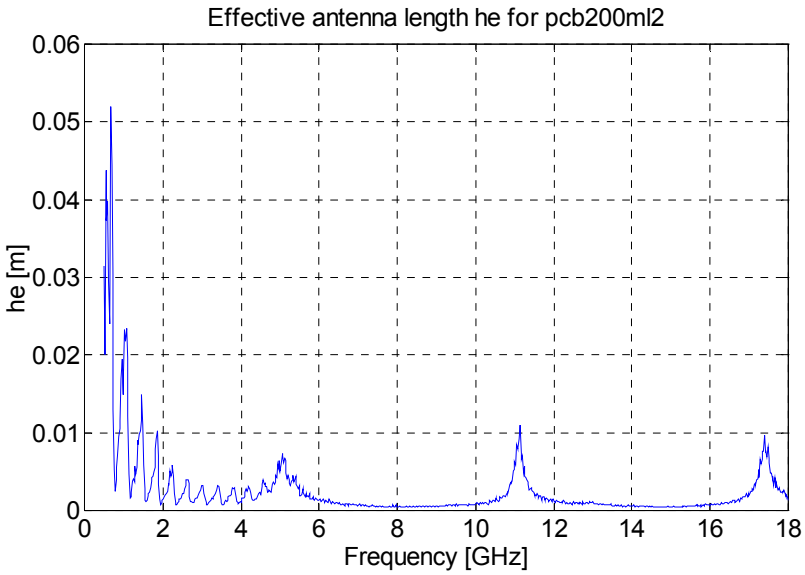

Fig. 7. Effective antenna length h_e for pcb200ml2

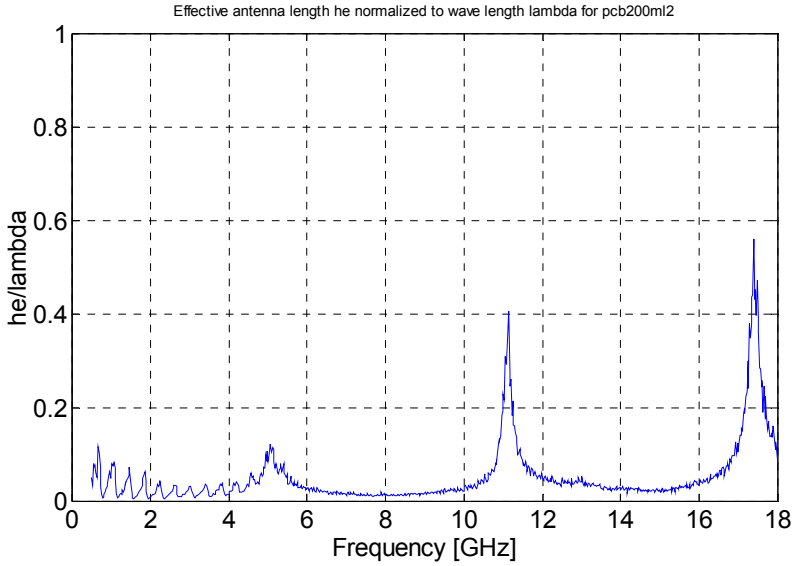

Fig. 8. Effective antenna length normalized to wavelength λ for pcb200ml2

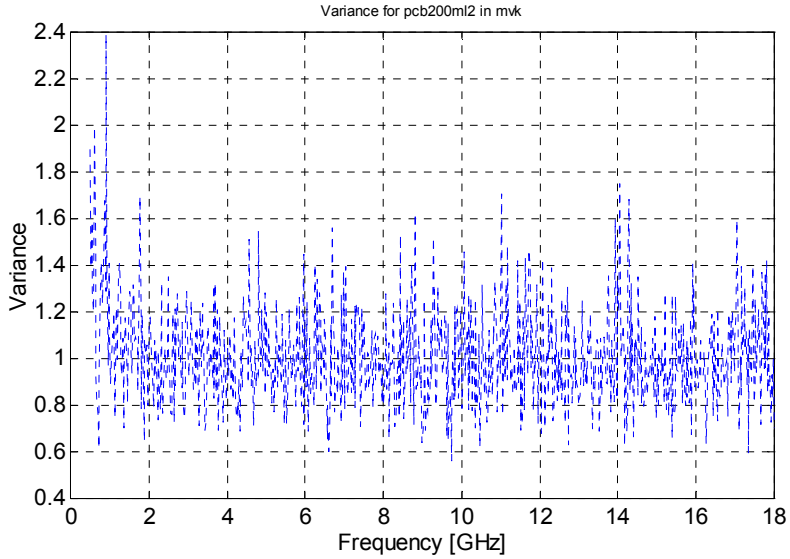

Fig. 9. Variance for pcb200ml2

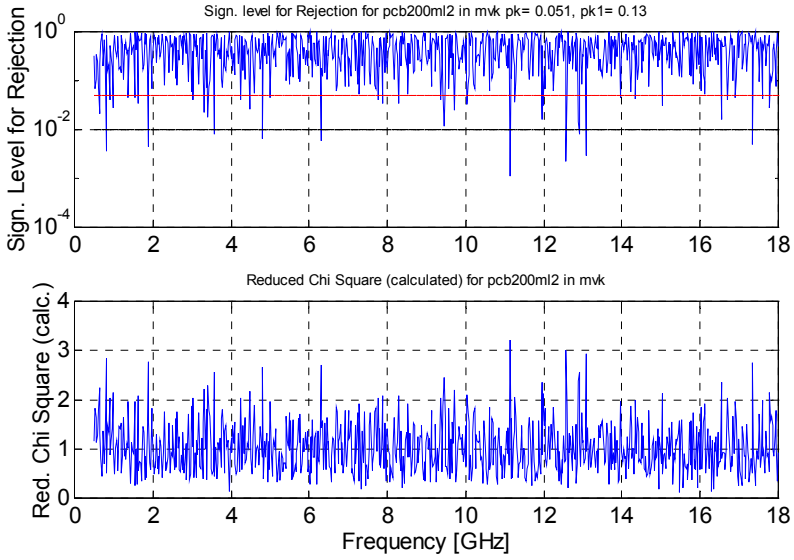

Fig. 10. Significance level for rejection (upper subplot) and the test variable ”Reduced Chi Square” (lower subplot) for pcb200ml2. p_k=0.051, p_{k1}=0.13

Microwave Field-to-Printed-Circuit-Board Measurements in Reverberation Chamber

Appendix G

Goodness-of –fit evaluation of a complete frequency interval.

(Adopted, with permission from the authors, from Appendix D in O. Lundén, M. Bäckström, and N. Wellander, *"Evaluation of Stirrer Efficiency in FOI Mode-Stirred Reverberation Chambers"*, FOI-R-0250—SE, November 2001, Swedish Defence Research Agency, Division of Sensor Technology, SE-581 11 Linköping, Sweden.)

A way to treat all the data for a complete frequency interval is to calculate a logarithmic sum of all the probabilities of rejection, p_i, given at each frequency. The sum is:

$$K = -2 \cdot \sum_{i=1}^{N} \ln(p_i)$$

where i denotes the frequency points and p_i is the probability of rejection at each frequency.

If the assumed distribution used in the goodness-of-fit test is true then each p_i is uniformly distributed. As an example, a goodness-of-fit test on, e.g., 1000 samples gives in such a case statistically 50 values of p_i that are smaller than 0.05, the 5 % rejection level.

Now define:

$$y = -2 \cdot \ln(p) \text{, where } y \in [0, \infty]$$

The cumulative distribution function is then given by:

$$F_Y(y) = P(-2 \cdot \ln X < y) = P(-y/2 < \ln X) = P(X > e^{-y/2}) = 1 - P(X < e^{-y/2}) = 1 - e^{-y/2}$$

(For an explanation, please see note below).

Which gives the frequency function:

$$f_Y(y) = \frac{1}{2} \cdot e^{-y/2}$$

thus

$$f_Y(y) \in \chi_2^2$$

i.e a χ^2- (chi-square) distribution with 2 degrees of freedom (DOF).

For $K = -2 \cdot \sum_{i=1}^{N} \ln(p_i)$ we then get that $K \in \chi_{2N}^2$

Note: $P(X < e^{-y/2}) = e^{-y/2}$. The reason for this is that since $y \in [0, \infty] \Rightarrow e^{-y/2} \in [0,1]$. Furthermore, since X is uniformly distributed we get that:

$$P(X < a) = a \Rightarrow P(X < e^{-y/2}) = e^{-y/2}$$